ADDIS ABABA UNIVERSITY

ADDIS ABABA INSTITUTE OF TECHNOLOGY

SCHOOL OF CIVIL AND ENVIRONMENTAL ENGINEERING



BOND BEHAVIOUR OF STEEL-CONCRETE CONNECTION OF BASES UNDER FATIGUE LOADING

A thesis submitted in partial fulfillment of the requirements for the degree of Master of Science in Civil Engineering

(Structural Engineering)

By

Tibebu Tesfaye

Advisor: Dr. Shifferaw Taye

March 2018

Addis Ababa

ADDIS ABABA UNIVERSITY

ADDIS ABABA INSTITUTE OF TECHNOLOGY

SCHOOL OF CIVIL AND ENVIRONMENTAL ENGINEERING

BOND BEHAVIOUR OF STEEL-CONCRETE CONNECTION OF BASES UNDER FATIGUE LOADING

A thesis submitted to the School of Graduate Studies of Addis Ababa University in partial fulfillment of the requirements for the degree of Master of Science in Civil Engineering (Structural Engineering)

By

Tibebu Tesfaye

March 2018

Approved by Board of Examiners

Dr. Shifferaw Taye		
Advisor	Signature	Date
Internal Examiner	Signature	Date
External Examiner	Signature	Date
Chair person	Signature	Date

UNDERTAKING

I certify that research work titled “Bond Behaviour of Steel-Concrete Connection of Bases Under Fatigue Loading” is my own work. The work has not been presented elsewhere for assessment. Where material has been used from other sources it has been properly acknowledged / referred.

_____

Tibebu Tesfaye

March 2018

ACKNOWLEDGMENTS

First and foremost I would like to thank the Almighty God for all his provisions.

My great pleasure is to my advisor, Dr.Shifferaw Taye. I am grateful of him for his encouragement from the very beginning, valuable suggestions and inspiration in guidance. I also express my gratitude to Dr. Abraham Gebre for his helpful comment and direction.

I also extend my gratitude towards my friends who in one way or the other helped me in accomplishing this study. In particular, I am very much thankful of Temesgen Abiy who was very helpful at all the critical moments. A friend in need is a friend indeed. I am greatly indebted to my beloved family for their help with great patience.

CONTENTS

ACKNOWLEDGMENTS i
List of Figures iv
List of Tables vi
List of Symbols vii
ABSTRACT viii
1 INTRODUCTION 1
1.1 Statement of the Problem 2
1.2 Objective 2
1.2.1 General Objective 2
1.2.2 Specific Objective 2
1.3 Significance of the Research 2
2 LITERATURE REVIEW 4
2.1 Bond Behaviour and Failure Modes 4
2.1.1 Factors Affecting Bond Between Steel and Concrete 7
2.2 Effect of Fatigue on the Steel Concrete Bond Behaviour 9
2.3 Fatigue in Concrete and Steel 10
2.3.1 Fatigue in Concrete Structures 10
2.3.2 Fatigue in Steel Structures 11
2.4 Finite Element Model 12
2.4.1 Finite Element Model of Concrete 12
2.4.2 Finite Element Model of Interface Surface 13
2.4.3 Finite Element Model of Bond 14
2.4.4 Finite Element Model of Reinforced Concrete 17
3 FINITE ELEMENT MODEL AND ANALYSIS 19
3.1 Introduction 19
3.2 Material Property Modeling of the Concrete 19
3.2.1 Compressive Behavior 19
3.2.2 Tensile Behavior 20
3.2.3 Concrete Damaged Plasticity Model 22
3.3 Damage Modeling 24
3.4 Material Behavior of Steel 25
3.5 Modeling the Bond at the Steel-Concrete Interface 26
3.6 Validation of Results 26

3.7 Summary of Development of Finite Element Model 30
3.8 Finite Element Analysis 32
4 RESULTS OF THE ANALYSIS AND DISCUSSION 33
4.1 Introduction 33
4.2 Effect of Concrete Strength 34
4.2.1 Effect on Bond Stress-Bond Slip Relation Under Monotonic Loading 34
4.2.2 Effect on Bond Stress-Bond Slip Relation Under Low Cycle Fatigue 37
4.3 Effect of Embedment Length 38
4.3.1 Effect on Bond Stress-Bond Slip Relation 38
4.4 Summary on the Effect of Concrete Strength and Embedment Length 41
4.5 Bond Stress-Slip Response for Cyclic Slip History 42
4.6 Bond Deterioration 42
4.7 Code Comparison 45
4.7.1 Eurocode Provision for Bond Strength 45
5 CONCLUSIONS AND RECOMMENDATIONS 48
5.1 Conclusions 48
5.2 Recommendations 49

List of Figures

Figure 2-1 Bond stress-slip curve for bar loaded monotonically and failing by pullout [1]. 5
Figure 2-2 Failure mode and bond stress-slip relationship....6
Figure 2-3 S-N curve for fatigue analysis.....10
Figure 2-4 Strain softening in the concrete structure.....11
Figure 2-5 Strain hardening in steel structures. 11
Figure 2-6 Schematic simulation of the idealized bond zone 15
Figure 2-7 Schematic representation of the bond element.....15
Figure 2-8 Tension stiffening behaviour in ABAQUS (adapted from ABAQUS 2006).....17
Figure 3-1 Compressive Stress-Strain Relationship for ABAQUS 20
Figure 3-2 Nayal and Rasheed's (2006) Tension Stiffening Model 21
Fig 3-3 Modified Tension Stiffening Model for ABAQUS.....22
Figure 3-4 Concrete damaged plasticity model 23
Figure 3-5 Post failure stiffness degradation damage properties of concrete 25
Figure 3-6a-Geometric parameters of concrete prism and steel rebar 27
Figure 3-7-Von-Mises stress result for validation model of this study 28
Figure 3-8 Validation result of the bond stress-displacement relation of different experimental and numerical result 29
Figure 3-9-Mesh for Finite Element Model of this study 30
Figure 3-10 Boundary conditions on FE model.....31
Figure 3-11 Flow chart of complete ABAQUS analysis 32
Figure 4-1 Finite Element model 33
Figure 4-2 Radial cracks at the initiation of bond cracks around steel-concrete interface 34
Figure 4-3 Bond stress slip curve of embedment depth L=30mm for varying concrete strength 34
Figure 4-4 Bond stress slip curve of embedment depth L=35mm for varying concrete strength 35
Figure 4-5 Bond stress slip curve of embedment depth L=40mm for varying concrete strength 35
Figure 4-6 Bond stress slip curve of embedment depth L=45mm for varying concrete strength 36
Figure 4-7 Bond stress slip curve of embedment depth L=50mm for varying concrete strength 36
Figure 4-8 S-N curve of short embedment (L=30mm) for varying concrete strength.....37

Figure 4-9 S-N curve of long embedment (L=50mm) for varying concrete strength 37
Figure 4-10 Bond Stress-Slip curve for varying embedment (fc'=20MPa) 38
Figure 4-11 Bond Stress-Slip curve for varying embedment (fc'=25MPa) 39
Figure 4-12 Bond Stress-Slip curve for varying embedment (fc'=30MPa) 39
Figure 4-13 Bond Stress-Slip curve for varying embedment (fc'=35MPa) 40
Figure 4-14 Bond Stress-Slip curve for varying embedment (fc'=40MPa) 40
Figure 4-15 Summary of bond strength for varying embedment length 41
Figure 4-16 Bond stress for varying concrete strength and embedment length 41
Figure 4-17 Bond degradation curves for varying concrete strength 43
Figure 4-18 Slip-number of cycle curves for varying concrete strength 44
Figure 4-19 EC-2 comparison with numerical results for different embedment length and concrete strength under monotonic loading.....46

List of Tables

Table 3-1 Compressive Stress-Strain Values for 40 MPa Concrete 21
Table 3-2 Comparison of experimental data with simulation results of the pulling the reinforcing rebar from the concrete block 29
Table 4-1-Maximum bond stress value for monotonic and cyclic slip history.....42
Table 4-2 Bond stress f_{bd} and basic anchorage length $l_{bd,\ reqd}$ for good bond conditions, fyk=400MPa 46
Table 4-3 Bond strength of numerical result after different cycles compared to EC-2 provisions (short embedment).....47
Table 4-4 Bond strength of numerical result after different cycles compared to EC-2 provisions (long embedment) 47

List of Symbols

Notations

A	Bearing area of the head of stud or anchor bolt
b_c	Coefficient for compression damage parameter
b_t	Coefficient for tension damage parameter
d_t	Damage parameter
E	Young's modulus
f_{bd}	Design value of the ultimate bond stress
f_{ctd}	Design value of concrete tensile strength
F_w	Wind force
f_{yk}	Characteristic yield strength of reinforcement
G_f	Fracture energy
L_b	Development length
$L_{bd,reqd}$	Required bond length
K	Stiffness values for a Traction(Stress) Separation
p_d	Dynamic pressure
t_s^o	Nominal traction stress vector
v	Wind velocity
∅	Diameter of the bar
β	Parameters depens on shape of stress strain diagram
ε_c	Compressive strain
ε_0	Strain corresponding to ultimate compressive stress
ε_d	Strain at descending portion of stress
η_1	Coefficient related to the quality of the bond condition
η_2	Reduction factor
ρ	Density of air
σ_{cu}	Ultimate compressive strength
σ_{sd}	Design stress of the bar at the position from where the anchorage

Abbreviations

EC2	Eurocode 2
ACI	American Concrete Institute
CDP	Concrete Damage Plasticity
FEM	Finite Element Method
FE	Finite Element

ABSTRACT

The base connections experiences stress reversals as a result of wind loading and can be subjected to bond degradation of steel-concrete connections due to fatigue loading. The study focused on the bond behavior of base connections of steel anchorages and concrete when subjected to fatigue loading. Fatigue loading can initiate cracks in the concrete surrounding the steel bars that propagate as the number of load cycles increases leading to the destruction of the concrete-steel interface and slip of the steel bars inside the concrete. This study investigated the effect of anchorage length and concrete strength on the bond behaviour of steel and concrete connection of bases subjected to monotonic and low cycle fatigue loading. The finite element analysis tool ABAQUS was used in this research to model the behavior of the connection and to study the bond behavior of the connection when subjected to fatigue loading. This model was then verified against other published numerical models and against different experimental tests performed in different laboratories. Once the model was considered representative an extensive parametric study was carried out. The result from this study illustrates the relationships between different parameters like concrete strength, embedment length and diameter of the steel and bond behavior. In steel concrete connection, design verifications for the bond of steel and concrete under fatigue load are required separately from monotonic loading. The fatigue behaviour of the bond between steel and concrete was not taken into consideration for current codes. Based on the parameters studied, repeated loading caused bond failure when subjected to a loading of as little as 76% of their static capacity.

Keywords: Finite Element Models; Bond (concrete–steel) stress; Damage Plasticity; Bond-Slip Relationship; Repeated Loading;

CHAPTER ONE

1 INTRODUCTION

Base connections of steel towers are subjected to several hundred million stress cycles caused by the turbulent nature of the wind. This causes low cycle fatigue, which could govern the design of the tower. This type of effect will be observed in slender structures subjected to wind loads such as transmission towers and traffic poles. One of the first fundamental facts of which human beings become aware is that nothing lasts forever. Life may come to a sudden end or last longer, but still for only a finite period. This latter case is normally supplemented by a reduction in efficiency, known as aging. This human life experience is directly reflected in materials science; under a high load a structure or a component can fail at once, whereas it can effectually sustain lower loads. On the other hand, the same structure or component can also fail under lower loads if they are applied over longer time frames in a constant (creep) or circular (fatigue) way.

Structures has to be anchored into the ground with a connection system that can withstand static, dynamic and fatigue effects of the environmental loads acting on the assembly and, as well as interaction effects generated and transmitted through the structure. Large load reversal can lead to bond degradation and damage accumulation resulting in bond failure, especially at the base connections where fatigue stress concentrations are generally high. The base (anchor bolts) are highly vulnerable to fatigue stress. Fatigue performance of anchor bolts connecting the flange at the base of the towers into a mass concrete base is the focus of this study.

Bond between steel anchorages and concrete element can be subjected to repeated or reversed loading. The fatigue phenomenon is analyzed by observing the increase in slip which indicates the progress of microcracking and microcrushing in the concrete. Slip increment depends on bond length and on parameters of the repeated load. The higher the load, the higher the slip increment. Slip increments decrease during the initial load cycles, and then slip increment is constant up to the maximum slip, at which the monotonic bond strength is reached.

1.1 Statement of the Problem

Major failures in the base connections of steel connections to concrete are due to critical cracks formed by accumulation of fatigue stress. Fatigue loading reduces the bond of concrete and steel and will eventually lead to failure. Thus, the area requires intact observation and researches from point of understanding bond behavior of connections under service life.

Code treatment of serviceability or fatigue limit state has been uneven and, in some instances, nonexistent. The drafting of national annexes to European codes is not finished and concerns only some part of actions and structures. Thus, different codes do not cover the broad domain of extreme actions.

The study is important for a more realistic assessment of the safety of steel anchored structures over its design life. Present bond seismic code provisions appear to be inadequate. These provisions are based on results obtained under monotonic loading, which are inadequate for judging the actual structural behavior under repeated loading.

1.2 Objective

1.2.1 General Objective

The main objective of the thesis was to assess bond behaviour of steel concrete connection of bases when subjected to fatigue loading.

1.2.2 Specific Objective

i. To study the bond behavior by varying different parameters of base connections.
ii. To develop a three dimensional finite element model capable of simulating the experimental bond-slip relationship between steel and concrete, thus providing an ability to study transfer of bond using finite element method.
iii. Studying the bond deterioration of steel concrete connection when subjected to fatigue loading.

1.3 Significance of the Research

The challenge faced when designing base connection system is on developing an accurate conception of all relevant phenomena. Repeated loading is one of the factors influencing bond behavior and it may produce premature failure. Varying loads on reinforced concrete elements stimulate an increase in crack widths, as the interface between steel bars and concrete “softens” under repeated loads. This study is intended to

improve understanding of the bond fatigue process. The significance of this study is that it will give the better understanding on the effect of repeated loading on steel-concrete connection bases. This will enable engineers and researchers to better understand the real behaviour of bond under repeated loading conditions.

CHAPTER TWO

2 LITERATURE REVIEW

2.1 Bond Behaviour and Failure Modes

The structural behavior of steel and concrete connected elements basically requires the interaction between steel and concrete. Tensile forces in the area of separating cracks and bending cracks are carried by the steel and transferred into concrete by bond action. Crack widths and crack spacing are therefore significantly dependent on the bond properties of the applied steel bars. Thus, stiffness and deformation behavior of composite elements are directly influenced by the bond properties.

A bond stress versus slip curve for a bar loaded monotonically and failing by pullout is shown in Figure 2-1[1]. Bond force and bond stress-slip curves, like bond strength, are structural properties that depend on both the geometry of the bar and the details of the concrete member, including the cover, transverse reinforcement, and state of stress in the concrete surrounding the reinforcement. As shown in Figure 2-1, bond force and bond stress-slip curves are initially very steep because of adhesion. Because of concrete shrinkage, which is restrained by the reinforcing bar, small internal cracks exist immediately adjacent to the reinforcing bar. These cracks can act as stress raisers and points of crack initiation at the bar ribs at relatively low loads. Because cracks tend to form in front of the ribs, small splitting cracks may begin to propagate from the ribs. If the reinforcing bar is placed in tension from a free surface, such as a beam-end specimen, it is possible for the crack to propagate to the surface, separating a roughly conical region of concrete from the rest of the specimen[2].

As loading continues, longitudinal splitting cracks will formed leading to a softening in the bond force-slip curve. In regions where these splitting cracks open and where confinement by transverse reinforcement is limited, the bar may slip with little local damage to the concrete at the contact surface with the bar ribs. In regions of greater confinement, higher rates of loading, or both, the concrete in front of the reinforcing bar ribs may crush as the bar moves, forming effective ribs with a reduced face angle. For higher values of confinement, all of the concrete between the ribs may crush or a shear crack may form along the periphery of the bar, or both, resulting in a pullout failure[1].

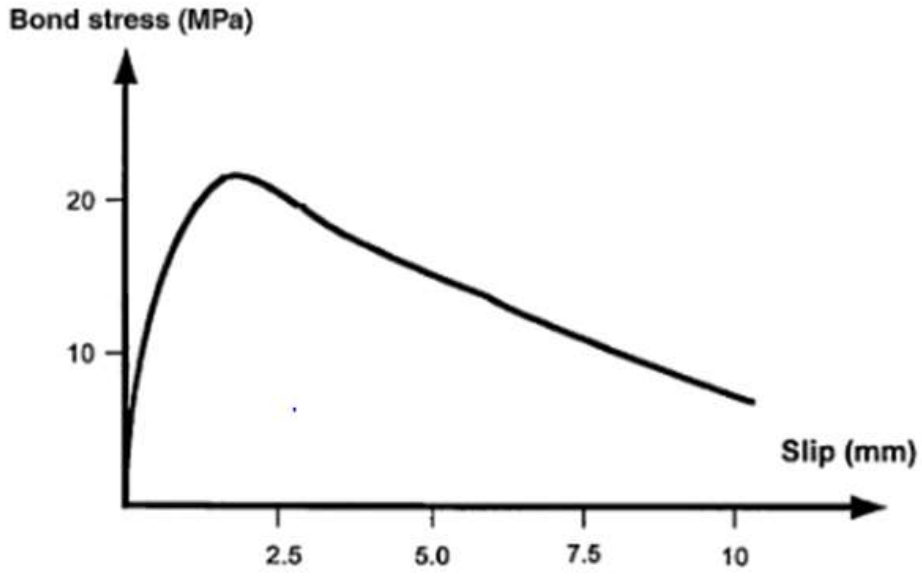


Figure 2-1 Bond stress-slip curve for bar loaded monotonically and failing by pullout [1].

For activation of the bond mechanism, relative displacements (slip) between steel and surrounding concrete are required. Essentially, bond action is achieved by mechanical interlocking of the steel ribs and the surrounding concrete. With initiating relative displacement, the ribs start to penetrate into the mortar matrix. The processes, which run in metallic materials, are not analogically transferable to a multi-phase, cyclic-loaded material such as concrete. However, the damage process seems to proceed similarly under cyclic and monotonic loading. Unloaded concrete already has micro-cracks between the cement matrix and aggregates. They occur due to the restrained shrinkage of the cement matrix caused by the aggregates. At sufficiently high loading, micro-cracks can occur in the cement stone.

The crack density of cyclically loaded specimens is higher than the crack density of monotonically loaded specimens. With further increase in load or load cycles, micro-cracks join and become macro-cracks, which eventually can lead to concrete failure without reinforcement[3]. Compressive stresses in the concrete compression struts additionally induce perpendicular tensile stresses and therefore inclined internal bond cracks starting at the ribs, so-called Goto-cracks [2], Figure 2-2.

The conical concrete compression struts are balanced by circumferential tensile stresses in the concrete cover. In case of exceeding this concrete tensile strength, cracking occurs longitudinal to the bar [2], see Figure 2-2 Depending on the confinement effect due to

the concrete cover or transverse reinforcement, these longitudinal cracks could result in splitting of the surrounding concrete, which comes along with an abrupt drop of the bond stress. This kind of bond failure is called splitting failure.

If adequate confinement of the bar is given by transverse reinforcement as well as high concrete covers, uncontrolled opening of these splitting cracks can be avoided and the bond strength can be increased further. With increasing tensile loading of the bar, the concrete teeth between the ribs are sheared off and the maximum bond strength is reached. With progressive slip the concrete teeth will be increasingly destroyed until complete shearing-off, as far as only frictional bond stresses between steel and concrete can be transferred. This bond failure mode is called pull-out failure.

The transition between the two failure modes generally depends on the bar surface, the position of the bar, the bar spacing, the transverse reinforcement and the concrete cover as well. In [4] the transition of splitting failure to pull-out failure is stated for related concrete covers of c/d = 2.5 to 3.5.

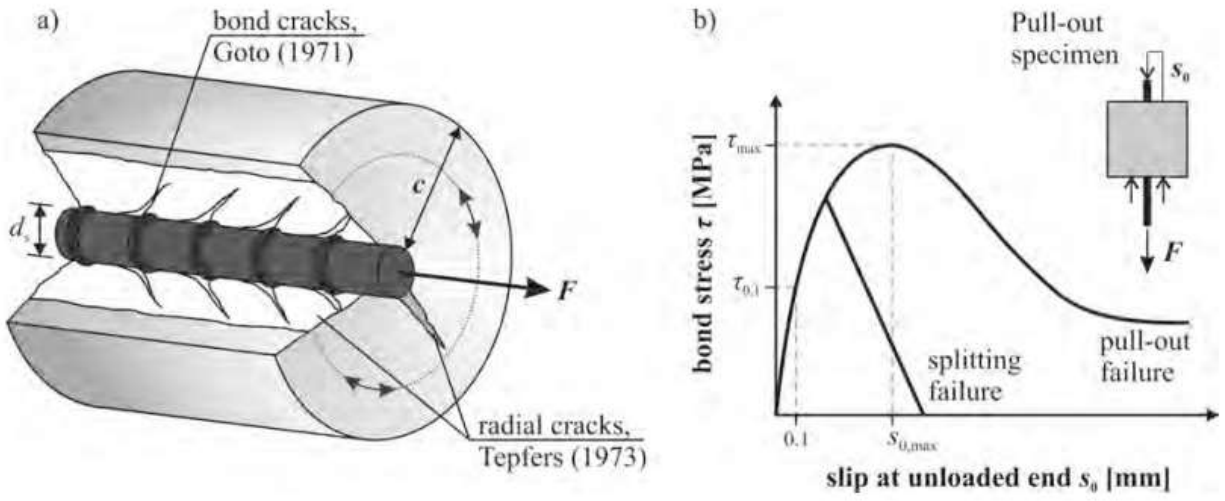


Figure 2-2 Failure mode and bond stress-slip relationship

In general bond stress-slip relationships are used to describe the bond behaviour, which can be determined on so-called pull-out specimens[5]. In real structural elements, bond stresses for large relative displacements are of minor importance. At this, the bond behaviour for small slip values, which correspond to the dimension of limiting crack widths, is relevant. Based on the assumption that the mean crack width in structural elements is approximately consistent with twice the slip at the unloaded bar end in pull-out tests, for the estimation of the bond behaviour in serviceability limit states the bond

stresses corresponding to slip values of s_0 = 0.1 mm are used, e.g. [5]. To characterize the bond behaviour, further parameters are the maximum bond stress max as well as the corresponding slip value s_0,max, which also can be taken directly from the bond stress-slip relationship, see Figure 2-2.

2.1.1 Factors Affecting Bond Between Steel and Concrete

2.1.1.1 Structural Characteristics

Concrete cover and bar spacing

Bond force-slip curves become steeper and bond strength increases as cover and bar spacing increase. The mode of failure also depends on cover and bar [2]. For large cover and bar spacing, it is possible to obtain a pullout failure. For smaller cover and bar spacing, a splitting tensile failure occurs, resulting in lower bond strength. The latter failure mode is the type expected to govern for most structural members. Splitting failures can occur between the bars, between the bars and the free surface, or both. Pullout-like failures can occur with some splitting if the member has significant transverse reinforcement to confine the anchored steel.

With bond failures involving splitting of the concrete for bars that are not confined by transverse reinforcement, the peak load is governed by the tensile response of the concrete, which depends on both tensile capacity and energy dissipation capacity, normally described as fracture energy G_f. Concrete exhibiting higher fracture energies provide improved bond capacities, even if the concrete has similar tensile strengths[6].

Development and splice length

Increasing the development or splice length of a reinforcing bar will increase its bond capacity. The nature of bond failure, however, results in an increase in strength that is not proportional to the increase in bonded length. The explanation starts with the observations that bond forces are not uniform and that bond failures tend to be incremental, starting in the region of the highest bond force per unit length. In the case of anchored bars, longitudinal splitting of the concrete initiates at a free surface or transverse flexural crack where the bar is most highly stressed. For spliced bars, splitting starts at the ends of the splice, moving towards the center. For normal-strength concrete, splitting may also be accompanied by crushing of the concrete in front of the ribs as the bar moves (or slips) with respect to the concrete. For higher-strength concrete and for normal-strength concrete in which the bars are epoxy coated, the degree of crushing in front of the ribs is significantly decreased. For splice specimens studied after failure, it is

common to see no crushed concrete at ribs near the tensioned end of a spliced bar, with the crushed concrete located at the end of the bar, indicating that failure occurred by a slow wedging action followed by rapid final slip of the bar at failure[7]. Because of the mode of bond failure, the unloaded end of a developed or spliced bar is less effective than the loaded end in transferring bond forces, explaining the non-proportional relationship between development or splice length and bond strength.

Although the relationship between the bond force and the bonded length is not proportional, it is nearly linear. Bars will have measurable bond strengths even at low embedded lengths. This occurs because, in the tests, there is always at least one set of ribs that forces the concrete to split before failure. When failure occurs, a significant crack area is opened in the member due to splitting [8]. As the bonded length of the bar increases, the crack surface at failure also increases in a linear but not proportional manner with respect to the bonded length. Thus, the total energy needed to form the crack and, in turn, the total bond force required to fail the member, increase at a rate that is less than the increase in bonded length. Therefore, the common design practice (ACI 318) of establishing a proportional relationship between bond force and development or splice length is conservative for short bonded lengths, but becomes progressively less conservative, and eventually not conservative, as the bonded length and stress in the developed or spliced bar increase.

Transverse reinforcement

Transverse reinforcement confines developed and spliced bars by limiting the progression of splitting cracks and, thus, increasing the bond force required to cause failure [2]. An increase in transverse reinforcement results in an increase in bond force, eventually converting a splitting failure to a pullout failure.

2.1.1.2 Bar Properties

Bar size

The relationship between bar size and bond strength is not always appreciated. The reason is that, while (1) a longer development or splice length is required as bar size increases, and (2) for a given development or splice length, larger bars achieve higher total bond forces than smaller bars for the same degree of confinement.

Addressing the second point first, for a given bonded length, larger bars require larger forces to cause either a splitting or pullout failure, for bars not confined by transverse reinforcement. The result is that the total force developed at bond failure is not only an increasing function of concrete cover, bar spacing, and bonded length, but also of bar

area [8]. The bond force at failure, however, increases more slowly than the bar area, which means that a longer embedment length is needed for a larger bar to fully develop a given bar stress (the first point).

When evaluated in terms of bond stress smaller bars appear to have even a greater advantage; thus, conventional wisdom suggests that it is desirable to use a larger number of small bars rather than a smaller number of large bars; this is true until bar spacing are reduced to the point that bond strength is decreased [2].

Steel stress and yield strength

For a number of years, concern existed that bars that yielded before bond failure produced average bond stresses significantly lower than higher strength steel in similar test specimens that did not yield[6]. As a result, test specimens were often deliberately configured to ensure that the bars did not yield prior to bond failure.

As it turns out, the bond strengths of bars that yield average only about 2% less when not confined by transverse reinforcement and about 10% greater when confined by transverse reinforcement than similar bars with the same bonded lengths made of higher strength steel that does not yield [6].

Bar surface condition

The surface of a reinforcing bar plays an important role in bond because of its effect on the friction between reinforcing steel and concrete and the ability of ribs to transfer force between the two materials. Bar surface condition involves the cleanliness of reinforcement, the presence of rust on the bar surface, and the application of epoxy coatings to protect the reinforcement from corrosion[9].

2.2 Effect of Fatigue on the Steel Concrete Bond Behaviour

Fatigue loading produces a progressive deterioration of bond that may lead to failure at cyclic bond stress levels lower than the ultimate stress under monotonic loading. Accumulation of bond damage is supposed to be caused by the propagation of micro-cracks[10] and progressive crushing [11] of concrete in front of the lugs. The bond between steel and concrete is an important parameter in determining the fatigue strength and the serviceability conditions. Despite its importance, the study of bond behaviour under repeated loading has not been given sufficient attention. Repeated loading causes failure of member by bond at lower loads than the static bond capacity. Microcracks in the concrete around the bars propagate as the number of cycles increases. This leads to the destruction of the concrete steel interface leading to slip of the bar [12].

Progressive deterioration of bond under repeated loading is observed in increasing slip[5]. Slip is significantly influenced by the load history. Important loading parameters are maximum and minimum levels of the repeated load, type of amplitude (constant or variable), frequency and sequence of amplitudes, type of load control(force or slip control) and number of load cycles. Deterioration of bond under repeated loading primarily depends on the peak slip (and not the peak stress) reached in the last cycle [7].

2.3 Fatigue in Concrete and Steel

2.3.1 Fatigue in Concrete Structures

Concrete fatigue is due to long term low amplitude force or stress, with many cycles occurring over the life of the structure that leads to concrete fracture. This can happen in tension, shear, and compression failure zones. Concrete fatigue is addressed by one internationally accepted code: FIB Model Code 2010, part of Eurocode 2. The basic tenets of fatigue analysis and analytical models are contained in this code. The principle of fatigue analysis relies on an empirical design model:

1. A stress-cycle (S-N) curve is developed based on cyclic fatigue load test data. This is the Envelope of Failure for the structure.
2. The analysis is based on summing the various fatigue loads to determine if the final structure "fits" within this Envelope.
3. The basic rule is the Palmer-Migren Summation or the Minor's Rule method of fatigue analysis.

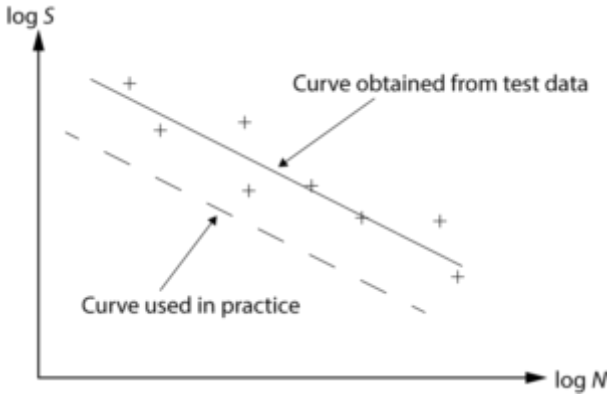


Figure 2-3 S-N curve for fatigue analysis.

With concrete material, the fatigue cracking is not physically visible; because concrete experiences a strain softening at high cycles, the crack propagation will continue un-noticed[15].

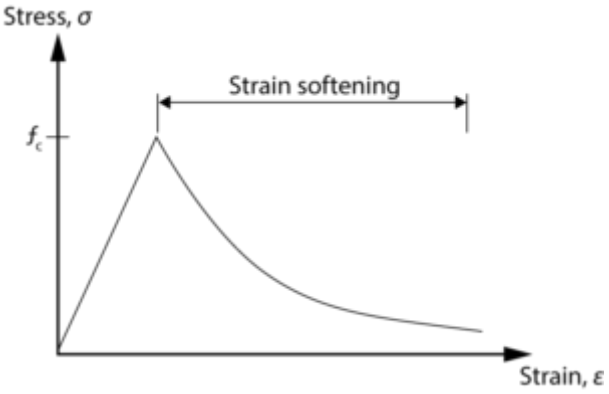


Figure 2-4 Strain softening in the concrete structure.

2.3.2 Fatigue in Steel Structures

Steel structures experience strain hardening with high cycle fatigue, so failure patterns are different. With steel, the critical points are stress concentrations, welds, and bolted connections[10].

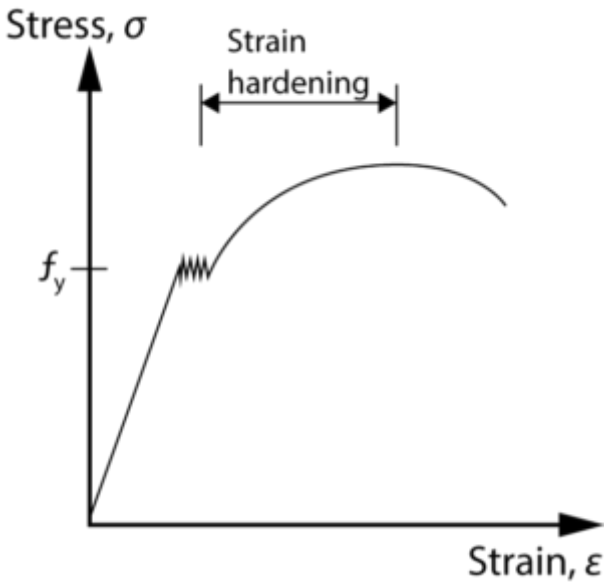


Figure 2-5 Strain hardening in steel structures.

2.4 Finite Element Model

2.4.1 Finite Element Model of Concrete

2.4.1.1 Cracking model

Cracking models define concrete property after yielding has occurred. The choice of material models of concrete is limited in Abaqus to the smeared cracking model, the brittle cracking mode and the damaged plasticity model [15]. Each model is designed for a particular type of usage. The smeared cracking model can handle only monotonic loading and low confining pressures. This sufficiently limits the range of its applicability. The damaged plasticity model is by far most complex concrete model incorporated in Abaqus that can be used in any loading regime. However, it is not 'user friendly', includes multiple parameters and its calibration can be very challenging.

Additionally, this model does not allow damaged elements to be deleted form the finite element (FE) analysis, which can lead to numerical instability of the solution algorithms. The brittle cracking model can be used in any loading regime and is very 'user friendly' and easy to calibrate. The main disadvantage of this model is that it assumes linear elastic material behaviour in compression. As a result, the model can be reliably used only in the cases where the concrete behaviour is dominated by the tensile failure[8].

The concrete smeared cracking model effectively reduces stiffness properties of the concrete over an area that has exceeded tensile yield stress. This smeared model does not track individual cracks but distributes the effects of these cracks. This model is most effective for use with concrete shell elements where reinforcement is typically defined in layers. The smeared cracking model does not take into account compression damage, but ultimate compression yield stress may be specified in the elastic properties. Since cyclic loading yields both compression and tension damage, the smeared cracking model is not ideal for seismic loading. The smeared cracking model will not be used for this model[13].

The concrete damaged plasticity (CDP) model uses stress/strain relationships to correlate parameters for relative concrete damage for both tension and compression. In a simple plasticity model after yielding has occurred, if force is removed, the residual plastic strain is found by a rebound function of the modulus of elasticity. Damage parameters of the CDP model modify this rebound function to include damage effects[16]. The CDP

model also accounts for cyclic loading effects where a recovery factor can be specified to account for the amount of total inverse loading strength available after damage has occurred. Thus, since this CDP model focuses on cyclic loading effects this model was chosen for implication into the final FEM [14].

The effects of these damage parameters change the inherent constitutive equations that are used to define the material properties each of individual element. As these constitutive equations change, the elements affected will in essence behave as a different material from concrete elements that have not yielded.

Typical values for compression recovery range from 0.85-0.99 while typical values for tension recovery range from 0.01-0.1. These typical values show that the compression cycle following a tension cycle will retain a significant fraction of total compressive strength[18]. This can be physically observed as cracks in the concrete close retaining compressive resistance. In contrast, a tension cycle following an extreme compression cycle where high compression damage has occurred would retain only a small portion of the ultimate tensile strength.

2.4.1.2 Tension Stiffening Relationship

In order to simulate the complete tensile behaviour of reinforced concrete in ABAQUS, a post failure stress-strain relationship for concrete subjected to tension is used which accounts for tension stiffening, strain-softening, and reinforcement interaction with concrete[19]. To develop this model, user should input young's modulus (E), stress, cracking strain values and the damage parameter values (dt) for the relevant grade of concrete.

2.4.2 Finite Element Model of Interface Surface

Connector elements

Connector elements are able to connect or join two different parts in Abaqus[15] with discrete geometry but having complex kinetic and kinematic relationships. These elements can have relative displacements and rotations local to the elements and are defined by individual attributes. Most single connector elements are able to describe a connection but connectors can also be used in parallel to describe complicated connection. Connectors available in Abaqus include:

1. Basic translational connectors with available translational degree of freedom at both nodes. The rotational degrees of the first of both nodes might also be available.

2. Basic rotational connectors with available rotational degree of freedom at both nodes.
3. Specialized rotational connectors with available degree of freedoms and also other degree of freedom at the nodes.
4. Assembled connectors which is a combination of the predefined basic translational and rotational connectors or translational and specialized rotational connectors.
5. Complex connectors with specialized degree of freedom at the nodes which cannot be defined by any individual connectors.

2.4.3 Finite Element Model of Bond

The numerical modeling of the bond behaviour is principally possible at two different levels: (1) detailed modeling (see Figure 2.6b) in which the geometry of the bar and the concrete is modeled by three-dimensional elements and (2) phenomenological modeling (see Figure 2.6c) based on a smeared or discrete formulation of the bar-concrete interface. In the phenomenological modeling of bond the concrete and the reinforcement are discretized by two- or three-dimensional finite elements[20]. The link between the bar and the concrete can be realized by a discontinuous approach where bond is defined by discrete, zero-thickness elements (springs) whose behaviour is controlled by the bond stress-slip relationship. This approach is able to realistically predict the bond behaviour for different geometries and for different boundary conditions only if a realistic constitutive model for the surrounding concrete is used. However, the model is not able to automatically predict the bond behaviour of a given bar geometry. Consequently, the influence of these parameters must be stored in advance in the basic parameters of the bond model. Thus one has the possibility to realistically simulate the behaviour of reinforced concrete structures with relatively low effort in modeling and computing time. By the use of detailed modelling, such as both modelling of the ribs of the reinforcement and the concrete lugs (see Figure 2.6b) between the ribs of the reinforcement a quite fine finite element mesh has to be generated[8]. This leads again to a high effort in modelling work and also to a really long computing time in particular while carrying out a finite element analysis on complex reinforced concrete structures.

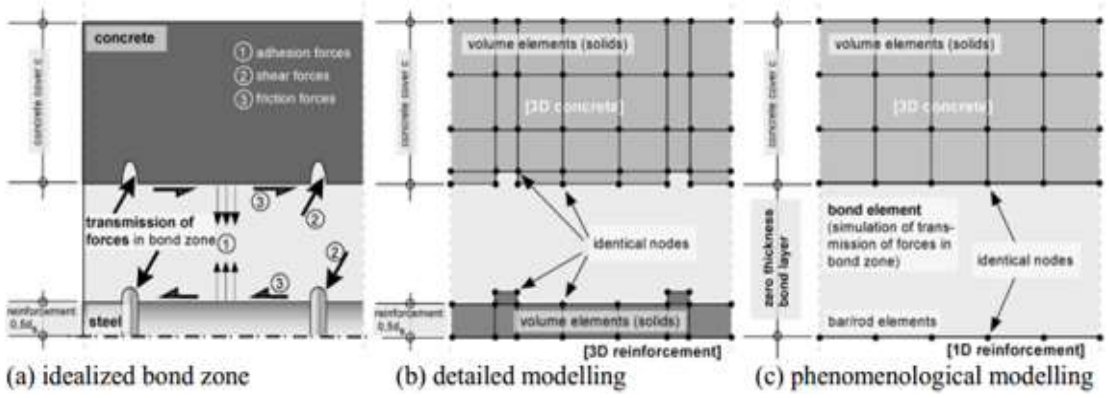


Figure 2-6 Schematic simulation of the idealized bond zone

The model used in the finite element code defines bond strength and stiffness as a function of the relative displacement (slip) between concrete and reinforcing steel. The bond element is incorporated into a finite-length and zero-width bond zone for the use in the three-dimensional finite element analysis of reinforced concrete structures (see Figure 2.7). It connects the one dimensional bar/rod finite element (reinforcement) with a three-dimensional concrete solid finite element. To determine the transmissible bond force only the slip in the bar direction is considered[21].

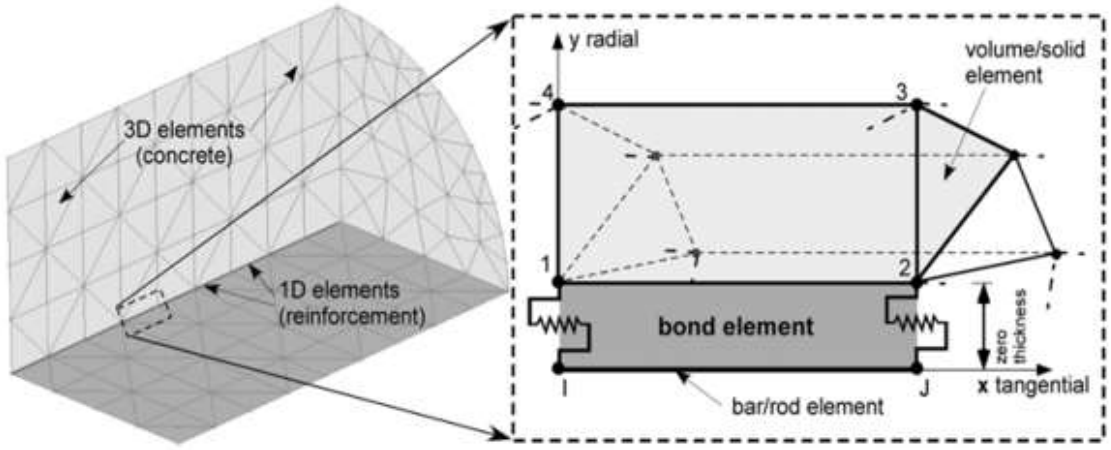


Figure 2-7 Schematic representation of the bond element

Based on the different FE models of concrete, there are various corresponding methods to represent the bond behavior. In a discrete concrete model, the bond may be considered as a contact problem between two different materials. Some dedicated elements have been developed to simulate this contact in earlier research and presently they are widely used in the commercial FE software. Some of these research efforts and the elements involved are described below.

In [21] developed a layered model to represent the bond. Because bond only occurs in concrete closest to the steel bar, they divided the concrete into two regions: an inner "boundary layer" and an outer layer of undamaged concrete. The thickness of the boundary layer was assumed to be 0.4 times the rebar diameter. The boundary layer was assumed to consist of a special homogenized material which included the bond slip relationship, instead of just normal concrete material. This layer was able to transfer the stress and displacement from the reinforcement to the concrete

A connecting element was first used by [9]. He introduced a double spring element to model the bond slip phenomena, as shown schematically in Figure 2.7.

This double spring element consisted of two springs, one acting parallel to the bar axis and one acting perpendicular to it [7]. These two springs were used to transmit normal and shear forces between the nodes of concrete and reinforcement. The springs were not considered to have dimension, and their stiffness were necessarily based on the characteristics of the bond slip relationship. In 1991, in the FE code ANSYS, the double spring element was modified into various possible unidirectional spring element configurations, as illustrated in Figure 2.7.

In the distributed concrete model, bond phenomena can be represented by a special property of the material, rather than by a connection, since the reinforcement is smeared into the concrete in the distributed model. In ABAQUS code, bond-slip is implicitly approximated by introducing some “tension stiffening” into the concrete model to simulate load transfer through the rebar. Tension stiffening is a bond-related behavior which decreases the tension in the steel due to bond, and increases the stiffness of the reinforcement, compared to that for a naked bar, after the RC cracks[22]. This is the nature of post-crack behavior for reinforced concrete in ABAQUS. The user can by inputting different tension stiffening parameters. The tensile behavior is defined as having elastic behavior until the stress reaches ultimate, the failure point of the material. Then, a linear or nonlinear softening model is used to represent post-cracking behavior including bond effect using the "tension stiffening" option of ABAQUS.

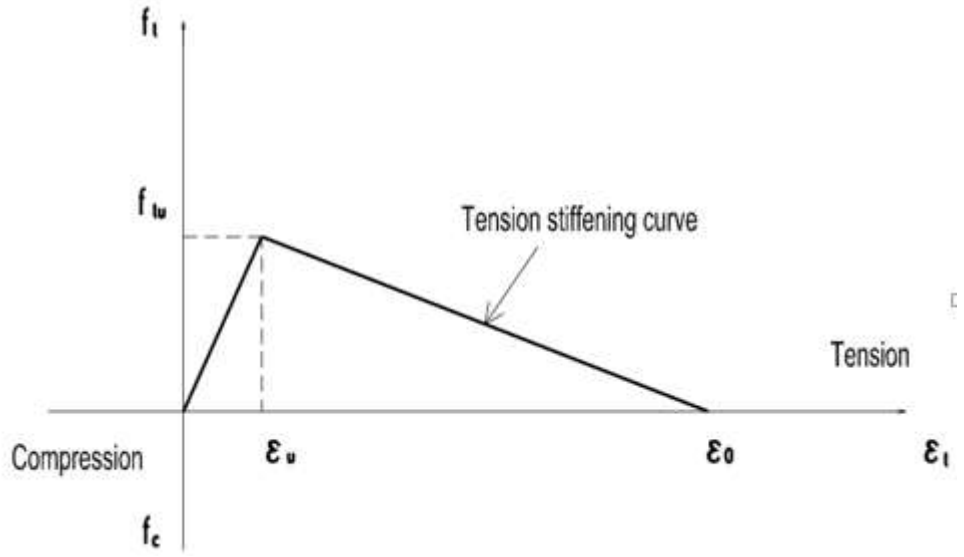


Figure 2-8 Tension stiffening behaviour in ABAQUS (adapted from ABAQUS 2006)

For the present study, a discrete reinforced concrete model was developed, and a complete bond-slip relationship, which included the nonlinear portion and the degradation for the bond simulation.

2.4.4 Finite Element Model of Reinforced Concrete

Unlike steel and aluminum, which have uniform constitutive properties, reinforced concrete consists of two totally different materials working together to resist various types of loadings. Therefore, it is somewhat complex to predict reinforced concrete behavior that includes the bond-slip relationship using the FE method. Currently there are three different FE models which are widely used to simulate reinforced concrete behavior. They are discrete, distributed and embedded models.

For the discrete modeling technique, separate, distinct elements are used to represent the concrete and the reinforcement. For instance, it is sometimes convenient to use a solid finite element to represent the concrete and to use a beam element to simulate the reinforcing bars. In the discrete model, concrete and steel are two totally independent parts[23]. For this modeling technique, special elements must be placed at the interface between the concrete and steel to represent the bond mechanism.

When using the embedded modeling technique, the rebar is considered as an axial member that is built into the concrete element. Because the rebar is embedded, the rebar has the same displacement as the concrete element. Perfect bond is assumed in this modeling technique, so that the two materials are assumed to work together completely as one unit.

When using the distributed modeling technique, the reinforcement is assumed to be smeared into every element of the concrete[24]. Compared to the embedded model, in which the contribution of the concrete and steel is calculated independently, for the distributed modeling technique, the rebar is transferred to an equivalent amount of concrete and the RC is considered as a homogeneous material in this model[25]. Perfect bond is again assumed for this technique.

Each of these three models has its own strong points[26]. The distributed model is frequently used in practical structural design and analysis, based on its simplicity of implementation. However, the internal force of the reinforcement is not available to be quantified in this model since the steel has been smeared. The discrete model is the only model of the three which can consider the bond slip mechanism directly, so it is very useful in more accurate RC simulations, despite the fact that the modeling process for this technique is the most complex. Moreover, it is more convenient to simulate irregular reinforcement in the discrete model, because the concrete and steel are separate entities.

CHAPTER 3

3 FINITE ELEMENT MODEL AND ANALYSIS

3.1 Introduction

A proper material model in finite element model which are capable of representing both elastic and plastic behavior of concrete in compression and tension have implemented. The development of a finite element model (FEM) may need intensive material testings to incorporate into the material model in any of the finite element [FE] packages available. There are quite large numbers of numerical material models available in the literature with potential to develop complete stress-strain curves of concrete for compression and tension separately based on experiment results. The most reliable model has incorporated which were applicable with the input format required for the finite element packages.

3.2 Material Property Modeling of the Concrete

3.2.1 Compressive Behavior

The complete compressive behavior should include both elastic and inelastic behavior of concrete including strain softening regimes. The complete stress-strain curve for concrete under compression is derived using the experimentally verified numerical method by [27]. This model can be used to develop the stress strain relationship under uni-axial compression up to 0.3 σ_{cu} of stress in the descending portion only using the maximum compressive strength (σ_{cu}). This method is briefly presented in the below section for the concrete with maximum compressive strength up to 40MPa. Figure 3-1 Compressive Stress-Strain Relationship for ABAQUS defines the ultimate compressive stress (σ_{cu}), strain at σ_{cu} (ε_0) and the strain corresponding to the stress at 0.3 σ_{cu} in the descending portion (ε_d). A linear stress-strain relationship which obeys Hooke's law is assumed up to 50% of the ultimate compressive strength (σ_{cu}) in the ascending portion. The numerical model by [27] is used only to calculate the compressive stress values (σ_c) between the yield point (at 0.5 σ_{cu}) and the 0.3 σ_{cu} in the descending:

$$\sigma_c = \left(\frac{\beta(\varepsilon_c / \varepsilon_0)}{\beta - 1 + (\varepsilon_c / \varepsilon_0)} \right) \sigma_{cu} \qquad (3\text{-}1)$$

where, the parameter β which depends on the shape of the stress strain diagram is derived from (3.2) and the strain at peak stress ε_0 is given by (3.3):

$$\beta = \left(\frac{1}{1 - \left[\sigma_{cu} / (\varepsilon_0 \, \mathrm{E}_o) \right]} \right) \tag{3-2}$$

$$\varepsilon_0 = 8.9x10^{-5} \sigma_{cu} + 2.114x10^{-3} \tag{3-3}$$

The initial tangential modulus, E_0 is given by:

$$E_0 = 1.24351x10^{2} \sigma_{cu} + 3.28312x10^{3} \tag{3-4}$$

Note: in the above equations, σ_c, σ_{cu} and E_0 are in kip/in^2 (Conversion factor: 1MPa=0.145037743 kip/in^2). The ε_d (strain at the 0.3 σ_{cu} in the descending portion) is iteratively calculated using when σ_c =0.8 σ_{cu}.

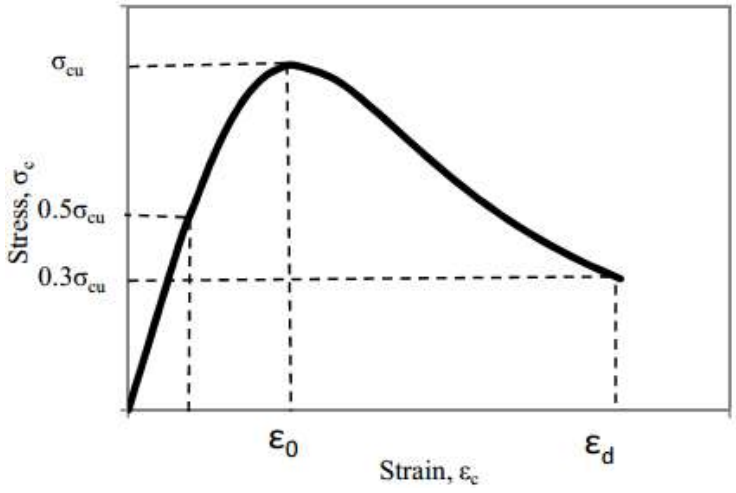


Figure 3-1 Compressive Stress-Strain Relationship for ABAQUS

3.2.2 Tensile Behavior

The model developed by [28] is selected for the present study as it is applicable for steel concrete elements with only minor changes. Also, this method indicates similarity to the tension stiffening model that is needed for ABAQUS concrete damaged plasticity model. This tension stiffening model was originally based on the homogenized stress-strain relationship developed by [29] which accounts for tension stiffening, tension softening and local bond slip effects. Two descending portions of the tensile stress strain graph has accurately captured the response caused by primary and secondary cracking phenomena [29]. The layered tension stiffening parameters used by [29] is replaced with a single set of stiffening parameters applicable to the entire tensile zone by the [27] to avoid the discontinuity in global response [27]. The [27] tension stiffening model for reinforced concrete elements is shown in Figure 3-2 Nayal and Rasheed's (2006) Tension Stiffening

Model and the modified tension stiffening model for the present study is presented in Fig 3-3 Modified Tension Stiffening Model for ABAQUS.

Table 3-1 Compressive Stress-Strain Values for 40 MPa Concrete

Stress (σ_c) N/mm^2	Inelastic Strain (ε_c^{in})	Damage (d_c)
2.56E+07	0.00E+00	0.00E+00
3.64E+07	1.00E-04	1.05E-02
4.49E+07	2.81E-04	2.95E-02
4.97E+07	5.87E-04	6.16E-02
5.12E+07	1.01E-03	1.06E-01
4.90E+07	1.76E-03	1.85E-01
4.43E+07	2.60E-03	2.73E-01
3.89E+07	3.46E-03	3.63E-01
3.37E+07	4.31E-03	4.53E-01
2.92E+07	5.14E-03	5.40E-01
2.54E+07	5.95E-03	6.25E-01
2.22E+07	6.74E-03	7.07E-01
1.95E+07	7.51E-03	7.88E-01

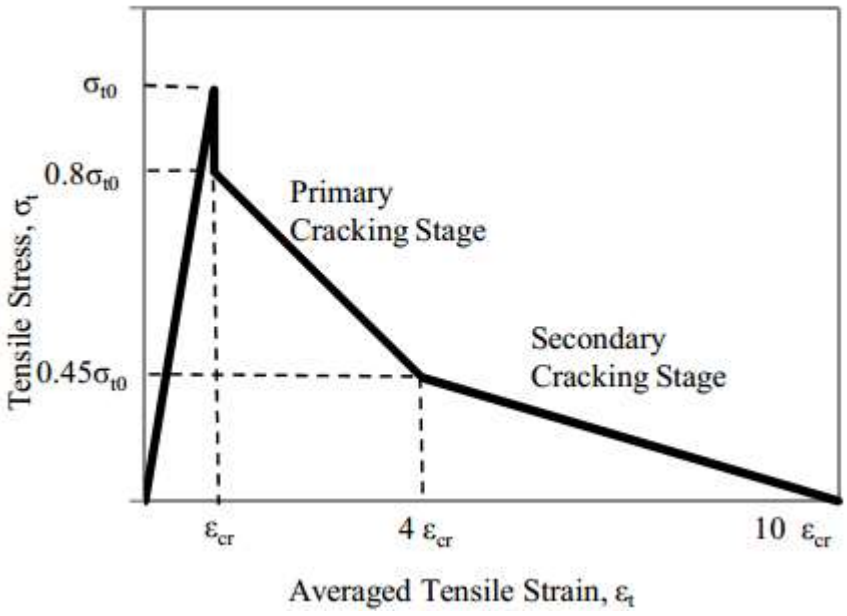


Figure 3-2 Nayal and Rasheed's (2006) Tension Stiffening Model

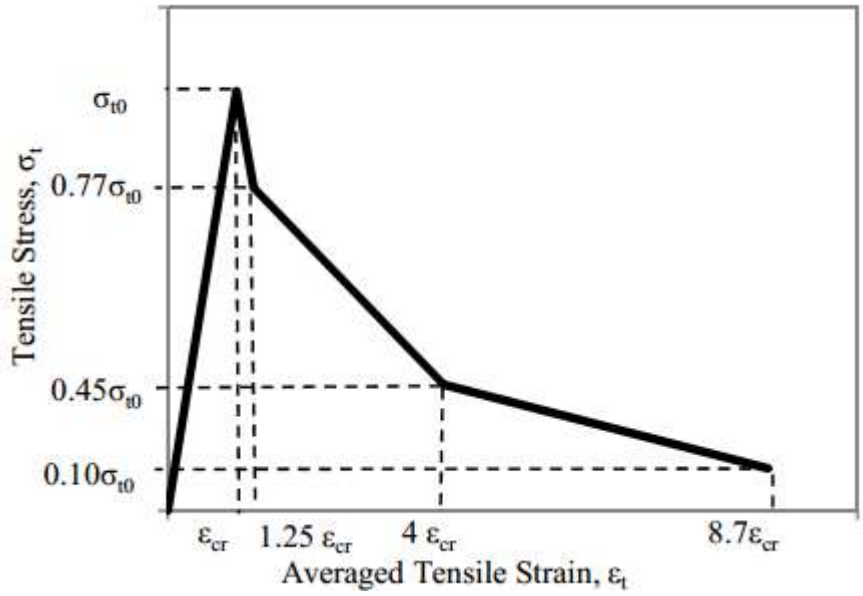
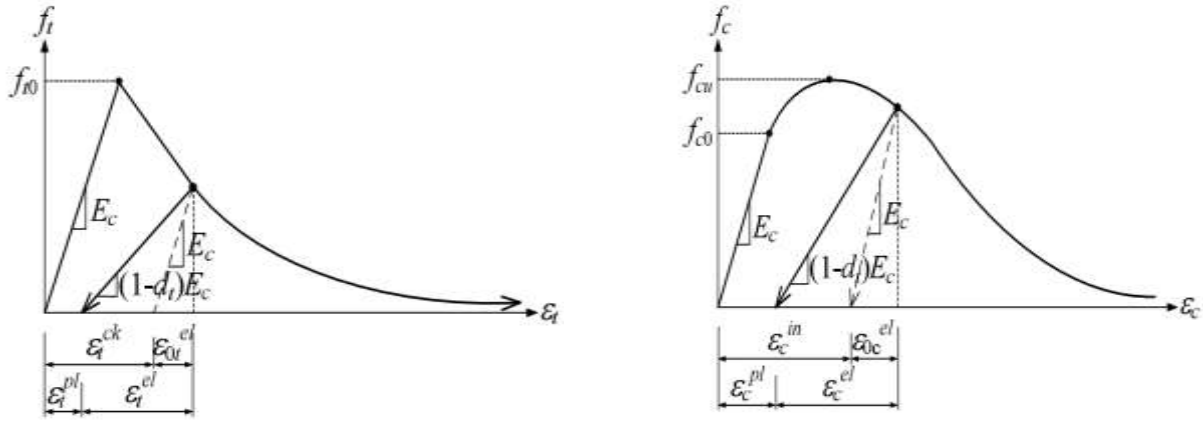


Fig 3-3 Modified Tension Stiffening Model for ABAQUS

3.2.3 Concrete Damaged Plasticity Model

The material model is a continuum, plasticity based, damaged model for concrete. Damaged plasticity is assumed to characterize the uniaxial tensile and compressive response of concrete as shown in Figure 3-4. At the beginning, the stress-strain relationship is linearly elastic under uniaxial tension until the value of the failure stress f_a is reached. Failure stresses in concrete block is converted to replace microcracks in it. Beyond the state of the failure stress in concrete, stress-strain response is designed by softening characteristic (Figure 3-4a).

Under uniaxial compression, the response is linear until the value of initial yield f_{c0}. After attaining the ultimate stress f_{cu} in the plastic zone, the response of concrete is characterized by the stress hardening followed by strain softening (Figure 3-4b).



(a) Tension behavior associated with tension stiffening

b) Compressive behavior associated with compression hardening

Figure 3-4 Concrete damaged plasticity model

Selection of parameters:

Since the calculations for these parameters involve complex mathematical derivations and assumptions using the yield surface of the concrete damage plasticity model, the proposed values in other researchers' work have been used here, and the verification of the model is performed by comparing the numerical results with published experimental data and is presented in below.

Dilation angle - A parametric study carried out suggested that there is not significant difference between 20° and 40° dilation angle if a reinforced concrete beam is subjected to bending. The best agreement with experimental data was reached for a dilation angle between 30° and 40° also performed a verification of this material model with experimental data, where a dilation angle of 31° was adjusted for uniaxial tensile and compressive failures, whereas a value of 25° was used for biaxial compressive failure. Hence, the dilation angle is selected as 31° in this work.

Flow potential eccentricity -The flow potential eccentricity is a small positive number, which defines the rate at which the hyperbolic flow potential approaches its asymptote [15] in the finite element simulation done by [16], the default value of 0.1 was used, which fitted the experimental test.

Ratio of biaxial to uniaxial compressive yield stress -The biaxial stress ratio and the tensile-to-compressive meridian ratio were assumed to be equal to 1.16 and 0.667.

Ratio of the second stress invariant on the tensile meridian -The ratio of the second stress invariant on the tensile meridian to that on the compressive meridian was taken as two-third (2/3).

Viscosity parameter -Since nonlinear material models with stiffness degradation often have convergence issues in ABAQUS, applying the technique of viscoplastic regularization is a common method to overcome this difficulty, which for sufficiently small amount of time increments, causes the consistent tangent stiffness of the softening material to become positive [15]. However, as suggested by [17], the selection of the value for the viscosity parameter affects the stiffness model, and a low value of the viscosity parameter should be selected (small compared to the characteristic time increment). The authors also performed parametric studies, and they found that the specimens with a viscosity parameter ranging from 0.00025 to 0.001 had good agreement with experimental results.

The bond damage initiation refers to the beginning of degradation of the cohesive response at a contact point. The process of degradation begins when the contact stresses and/or contact separations satisfy certain damage initiation criteria.

3.3 Damage Modeling

Damage is generally characterized by the reduction of elastic constants. Both the reduction of unloading stiffness and unrecoverable deformation have been clearly observed in concrete compression tests [13,15] as illustrated in Fig. 2, which suggests that the concept of plasticity should be combined with the concept of damage to correctly represent the nonlinear behavior of concrete. Damage parameters take values ranging from 0 (no damage) to 1 (fully damaged), representing the level of damage.

$$d_c = 1 - \frac{\sigma_c E_c^{-1}}{\varepsilon_c^{pl}(1/b_c - 1) + \sigma_c E_c^{-1}} \quad \textbf{(3-5)}$$

$$d_c = 1 - \frac{\sigma_t E_c^{-1}}{\varepsilon_t^{pl}(1/b_t - 1) + \sigma_t E_c^{-1}} \quad \textbf{(3-6)}$$

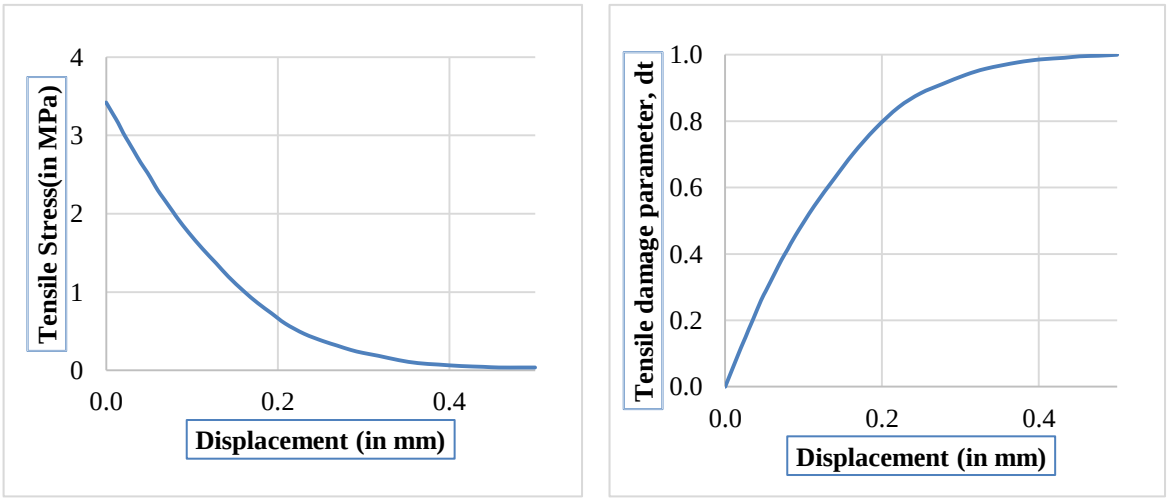
Description of these parameters can be found in Fig. 3.4. The coefficients bc and bt take values between 0 and 1 and for this study bc=0.7 and bt=0.1 is used [10]. In different pushover analysis simulations, bc=0.7 and bt=0.4 were found to produce a convergent solution.

Damage parameter contour maps in tension and in compression are utilized for the visualization of tensile cracks as well as crushing regions. It is not possible to draw discrete crack locations since the cracks are smeared through solid finite elements.

Stiffness Recovery

Default values for stiffness recovery factors are assumed in the present study. Therefore, the compressive stiffness recovery factor, w_c = 1 is used assuming that compressive stiffness is fully recovered upon crack closure as the load changes from tension to compression and the tensile stiffness recovery factor, w_t= 0 is used assuming that tensile stiffness is not recovered as the load changes from compression to tension once crushing of concrete is initiated.

The stiffness degradation damage caused by tensile failure (cracking) of the concrete dt is used as shown in Figure 3.5(b) with compression recovery factor 0. The stiffness degradation damage due to the compressive crushing dc is assumed to be 50% for



corresponding strain 0.001375 with tension recovery factor 0.8.

a) Stress-displacement relation **b) Tension damage model**

Figure 3-5 Post failure stiffness degradation damage properties of concrete

3.4 Material Behavior of Steel

Steel of the reinforcing bars has approximately linear elastic behavior when the steel stiffness introduced by the Young's or elastic modulus keeps constant at low strain magnitudes. However, once the stress in the steel exceeds the yield stress, permanent

(plastic) deformation begins to occur. The stiffness of the steel decreases once the material yields. The plastic deformation of the steel material increases its yield stress for subsequent loadings.

The yield and ultimate strengths were taken for longitudinal steel bars are 355 MPa and 510 MPa with Young's modulus of elasticity, *Es* = 21000GPa and Poisson's ratio, v= 0.3.

3.5 Modeling the Bond at the Steel-Concrete Interface

The steel-concrete interface was modeled by interface elements available within the ABAQUS [15] element library. Interaction between the steel and concrete surfaces is modeled using friction formulation in tangential direction and hard contact in normal direction to avoid penetration into each other. The penalty method is used for tangential behavior along with the coefficient of friction as 0.8. For normal interaction, hard contact option is used and the separation was allowed after contact in the interaction model. The method requires defining two surfaces that are the master and slave surfaces. In modeling the steel-concrete interface, the master surface within the model was the steel anchors and the slave surface was the concrete. The interface elements are formed between the master and slave surfaces and monitor the displacement of the slave surface in relation to the master surface. When the two surfaces remain in contact, the slave surface can displace relative to the master surface based on the coefficient of friction between the two surfaces.

3.6 Validation of Results

Successful finite element models are those validated against sufficient number of tests, preferably from different sources. Finite element modeling can be extended, once validated, to conduct parametric studies investigating the effects of the different parameters affecting the behavior of steel and steel-concrete composite bridges. The analyses performed in the parametric studies must be well planned to predict the performance of the investigated outside the ranges covered in the experimental program. The parametric studies will generate more data that fill in the gaps of the test results and will help to understand the performance under different geometries and scenarios. Hence, one of the advantages of the finite element modeling is to extrapolate the test data.

Validation of Bond Between Steel and Concrete Block with Account of Friction and Concrete Damage

Experiment

The comparison of obtained results of finite element simulations with experimental data done by RILEM/CEB/FIB [27] Recommendation on reinforcement steel for reinforced concrete pull-out tests (1983) is presented and discussed for the problem of pulling the reinforcing bar from the concrete block. Loading conditions and geometric parameters are shown in Fig. 3.6a and 3.6b.

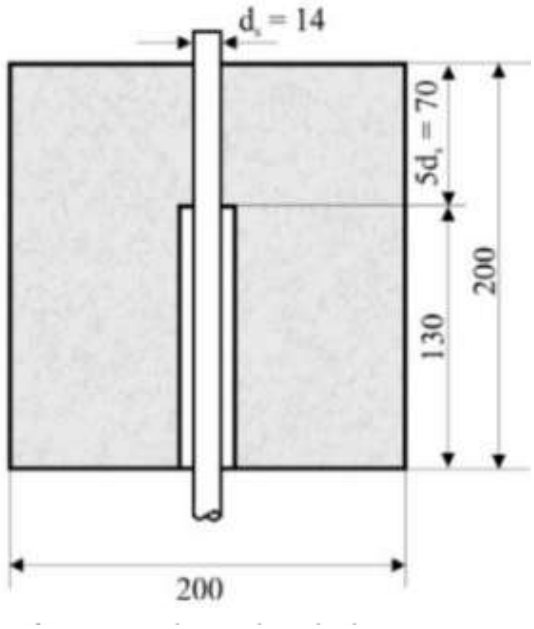


Figure 3-6a-Geometric parameters of concrete prism and steel rebar

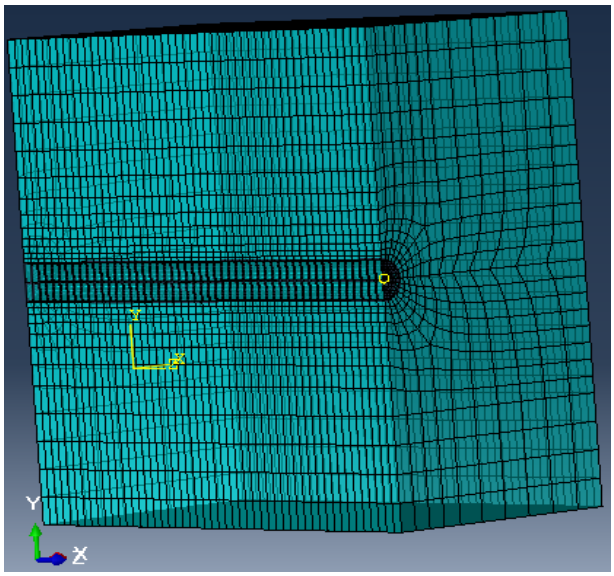


Figure 3-6b-Finite element model for validation

Pull-out test experiment was conducted on tensile tester Shimadzu AG-300kN [A.V. Benin, A.S. Semenov, S.G. Semenov, B.E. Melnikov, MCE, 5, 86-144 (2013)]. Steel reinforcement Ø14 and concrete C-25 were used in experiments.

Modeling

The elastic, elastic-damage and elastic-plastic damage models are used in the present analysis for the concrete model. In order to capture the degradation of the elastic stiffness of the concrete material as well as its irreversible deformations upon mechanical loading, the combined use of elastic-plastic constitutive equations along with continuum damage mechanics became vital to better describe the mechanical behavior of concrete.

Cohesive behavior was used to describe destroying of reinforced-concrete bond. The available traction-separation model assumes initially linear elastic behavior followed by the initiation and evolution of the bond damage.

The results of simulation of the pulling the reinforcing bar from the concrete block (see Fig. 3.7) are obtained using axisymmetric finite element(FE) model (FE mesh is shown in Fig. 3.6b). The numerical model consists of 8-node quadrilateral elements (CAX8R). The computations were performed using the FE software package ABAQUS [14].

Material parameters used in simulations are: concrete compression strength fc' =18.5 MPa, tensile strength, fctk= 1.55 MPa, Young modulus is E =30000 MPa, Poisson's ratio is & = 0.2. To describe linear elastic traction-separation behavior the following parameters were used: Knn=1500 MPa/mm, Kss =360 MPa/mm, and Ktt =360 MPa/mm.

Maximum stresses, which were used for damage initiation, are: t_n^o =110 MPa, t_s^o =9 MPa, and t_t^o =9 MPa. The elasticplastic model with isotropic hardening [23] with σ_{02} =235MPa is used for steel rebar in FE computations.

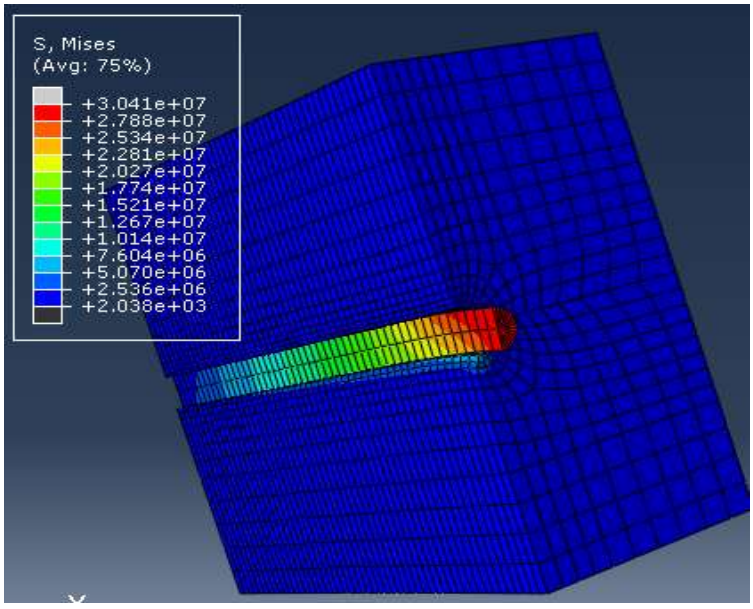


Figure 3-7-Von-Mises stress result for validation model of this study

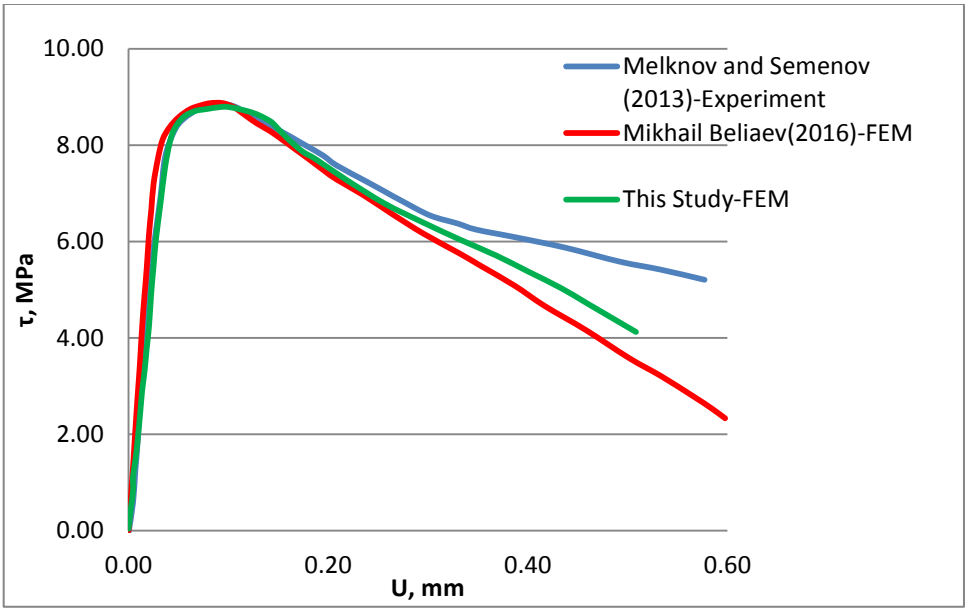


Figure 3-8 Validation result of the bond stress-displacement relation of different experimental and numerical result

The simulation result is shown in Fig. 3.7. It is observed that the load-displacement curves from the two numerical studies are almost identical up to maximum shear is obtained.

Table 3-2 Comparison of experimental data with simulation results of the pulling the reinforcing rebar from the concrete block

S.N		Maximum shear stress in bond (Mpa)	Convergence to Experiment result (%)
1	Experiment	8.888	0
2	Finite Element Model	8.790	1.097
3	Numerical Model by Mikhail Beliaev	8.871	0.084

Beyond that point, cracking is initiated, and the two simulations diverge until the peak load, which is also almost the same. The post-peak unloading, during which the cohesive elements become completely damaged, occurs at a much lower load in the present study when compared to experimental study. But approximation when compared with finite element model studied by Mikhail Beliaev (2016). This is probably related to the much coarser mesh used and the cohesion and plastic damage model included in the present study.

The corresponding experimental result reported by Melnikov and Semenov is also plotted along with the two numerical simulations in Fig. 3.8. Good agreement is obtained

up to the peak load. The post-peak behavior shows differences primarily due to the poor calibration of results for idealizing damage parameters.

Considering the overriding practical importance of the peak load, rather than of the softening region, the results obtained from the simulation approach followed in the present study are deemed to be adequately accurate as well as computationally efficient.

3.7 Summary of Development of Finite Element Model

Element

For modeling of concrete and steel, solid element is chosen. In general, second-order solid elements are more efficient for complex geometric and stress displacement modeling. In a reduced integration analysis procedure, first-order element acquires potentially stiffer behaviour with a slow convergence rate, preventing mesh locking and complexity. Hence, an incorporated reduced integration with the first-order 3D 8-node solid element (C3D8R) is used for steel and concrete to overcome the possible errors and to consider the cracks in tension. Such elements require a denser mesh for efficient and precise geometric simulations.

Mesh

Accuracy of the results basically depends upon the finite element mesh size and type. Different mesh sizes were tried prior to converging at the final FE mesh which is shown in Figure 3.9.

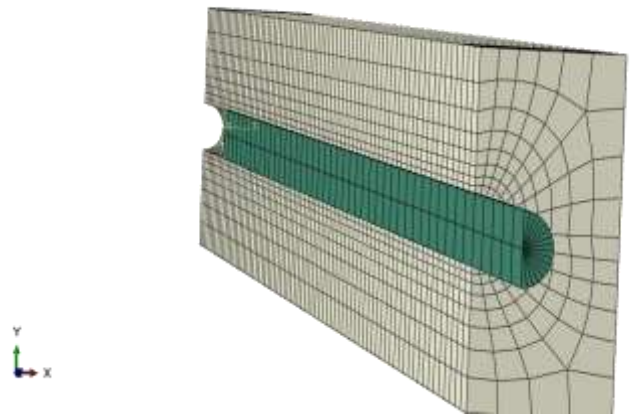


Figure 3-9-Mesh for Finite Element Model of this study

The model is meshed with approximate element size with 10mm x 10mm x 10mm in longitudinal, transverse and thickness direction respectively. Mesh convergence study

carried out using displacement measurements depicts that the above mesh is finer enough to obtain a reliable result. Because of analytical constraints the mesh size could not be reduced beyond 10 mm.

Boundary Conditions

In order to save the CPU and time of analysis, only one quarter of the specimen was modeled, as shown in Figure 3-10 Boundary conditions on FE model by taking advantage of the symmetry of the element by introducing a symmetry boundary condition along the X-symmetric axes of the model.

At the bottom of the model "ENCASTRE" was specified means fully built-in (fixed case), which implies that the degrees of freedom 1, 2, 3, 4, 5, and 6 equal to 0.

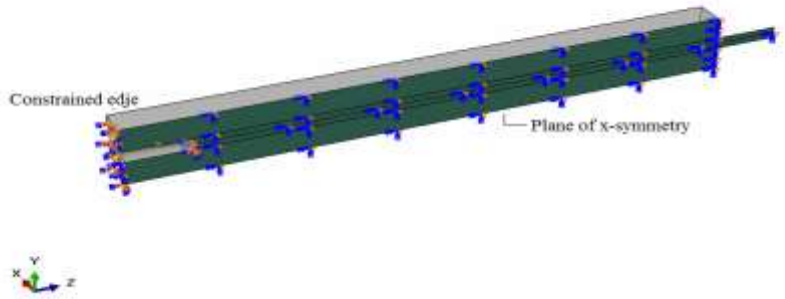


Figure 3-10 Boundary conditions on FE model

Step Time Definition

The quasi-static implicit model is set for static, using a general time step for the time period of 1 second. The geometric non-linearity (Nlgeom) option is used to model the non-linearity accurately. The maximum number of increments is specified to 2000. The initial time increment is assigned to 0.01, the minimum time increment to 1×e−8 and the maximum time increment to 0.01.

3.8 Finite Element Analysis

The first step of a finite element analysis using ABAQUS is to discretize the actual geometry of the structure using a set of finite elements for defining the model of the physical problem and to create an ABAQUS input file. In this study, model is created graphically using preprocessor software ABAQUS/CAE (2004), which is a complete ABAQUS environment that provides a simple, consistent interface for creating, submitting, monitoring, and evaluating form ABAQUS/Standard and ABAQUS/Explicit modeling process. Defining the geometry and material properties, as well as generating a mesh are done by moving from module to module and developed a model to generate an input file. However, the input file generated by ABAQUS/CAE is altered later for defining properties and parameters that are not supported by ABAQUS/CAE using a text editor. A complete analytical procedure in ABAQUS usually consists of three stages: i) Preprocessing, ii) Analysis, and iii) Post processing. The sequential progress of these three stages is shown in Figure 3.11.

The linear static analysis was performed by ABAQUS/Standard in only one increment; however, the ABAQUS/Explicit (2004) requires a large number of increments because very small increment of time is required to get the stable solution of equation of motion and keep the stability limit. The total execution time of the explicit analysis was taken 4 hours 15 minutes.

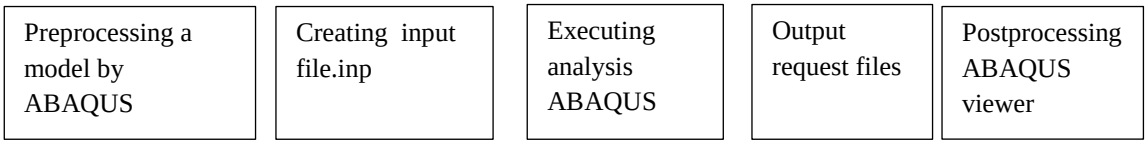


Figure 3-11 Flow chart of complete ABAQUS analysis

CHAPTER 4

4 RESULTS OF THE ANALYSIS AND DISCUSSION

4.1 Introduction

The parameters used in the study are chosen based on the assumption that they will have an influence on the bond behaviour of a steel-concrete column base connection. There are many different types of parameters to study, it is however reasonable to assume that certain parameters have a larger influence on the bond behavior under fatigue loading than others, this thesis focused on the effect of varying concrete strength and embedment length.

In order to save the CPU and time of analysis, only half of the element was modeled, as shown in Figure 4-1 Finite Element model by taking advantage of symmetry of the sample by introducing a symmetry boundary condition along the vertical symmetric-axes.

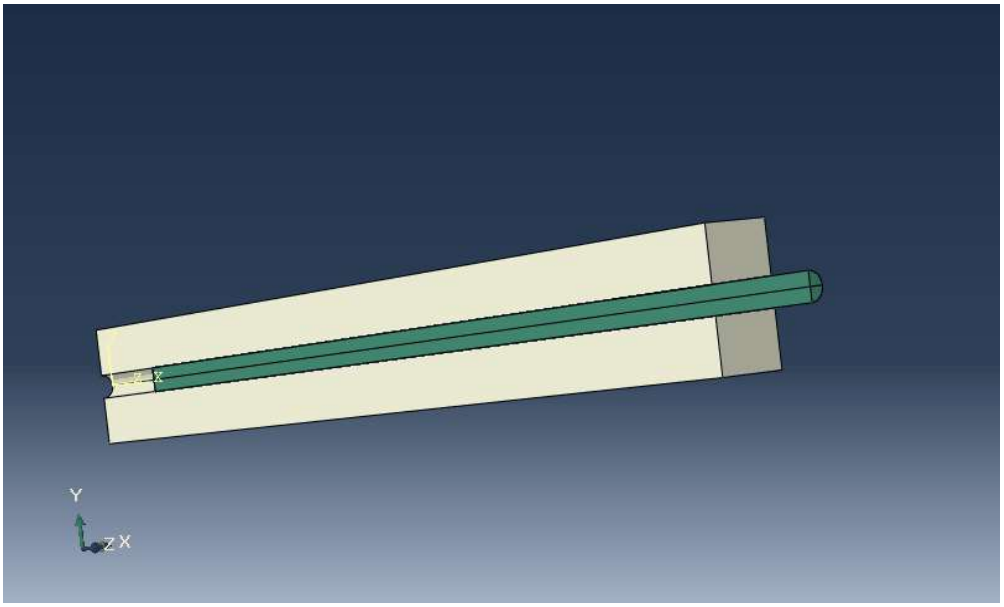


Figure 4-1 Finite Element model

Note that an unbonded length of 10db is provided at the loaded end of the bar to eliminate the effect of end conditions on bond response. The dimensions of the anchorage block are chosen to provide sufficient concrete cover to preclude a splitting-type bond failure and sufficient anchorage length to ensure yielding of the anchorage bar. Tensile fatigue load is applied to the exposed end of the anchorage bars.

Abaqus uses the programming language Python for scripting and have built-in Python scripts that contain commands to define parameter studies and allows to generate,

execute and gather the results from the simulations in an effective manner. This is done by creating a parametrized input file containing a parameter definition and a parameter usage, developing a .psf file containing the script which executes the parameter study. The Python script is presented in Appendix A. In the statistical evaluation, the simulations must include every possible combination of the varying parameters.

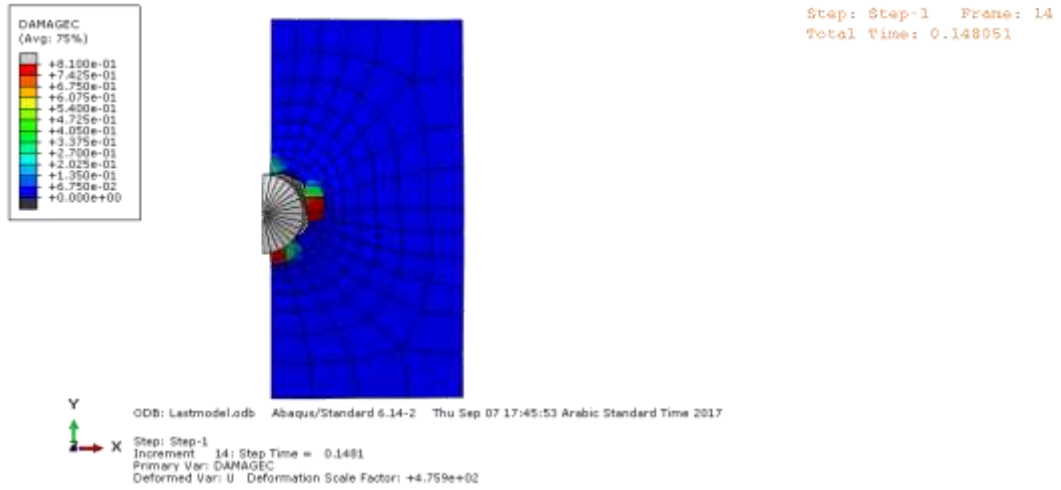


Figure 4-2 Radial cracks at the initiation of bond cracks around steel-concrete interface

4.2 Effect of Concrete Strength

4.2.1 Effect on Bond Stress-Bond Slip Relation Under Monotonic Loading

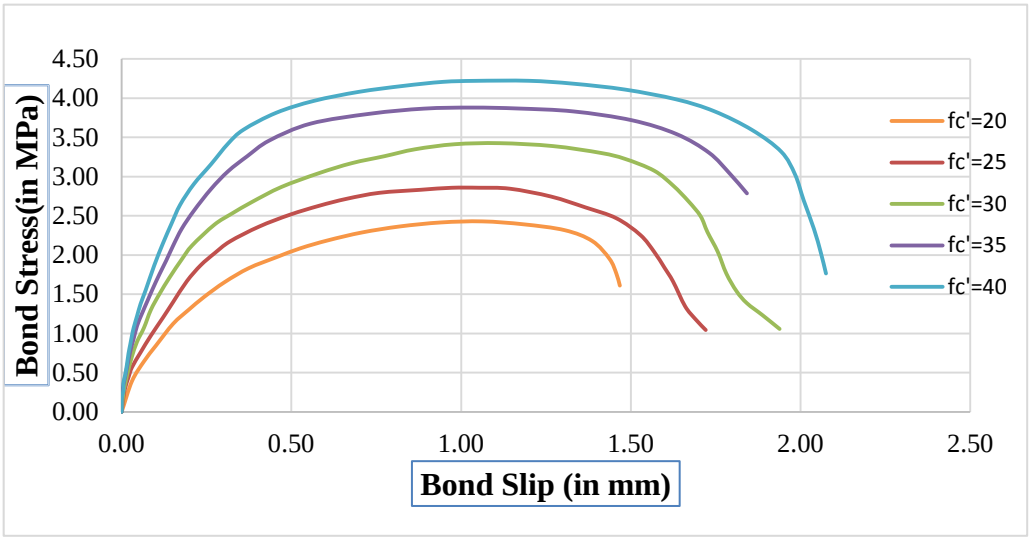


Figure 4-3 Bond stress slip curve of embedment depth L=30mm for varying concrete strength

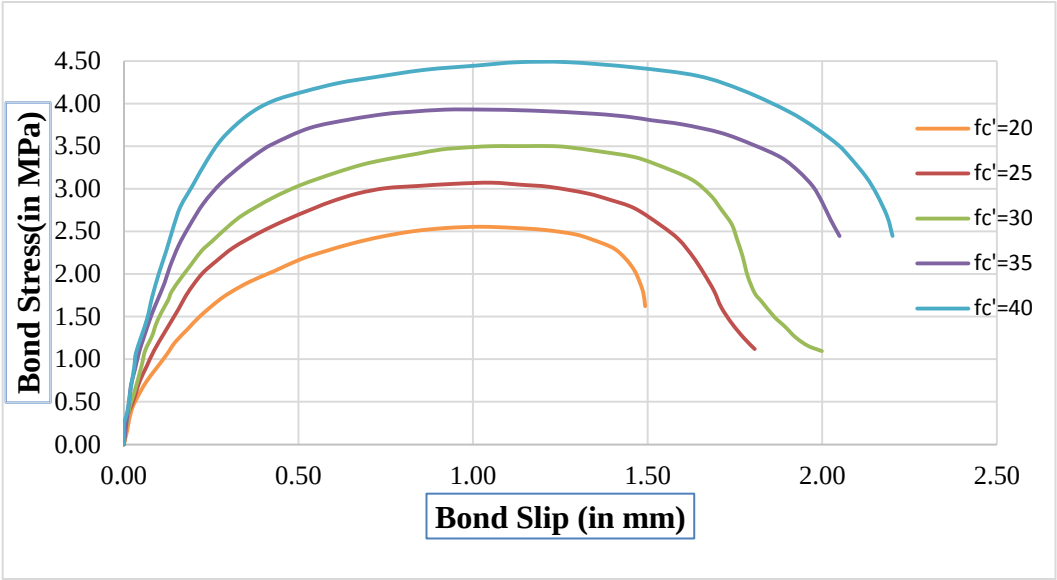


Figure 4-4 Bond stress slip curve of embedment depth L=35mm for varying concrete strength

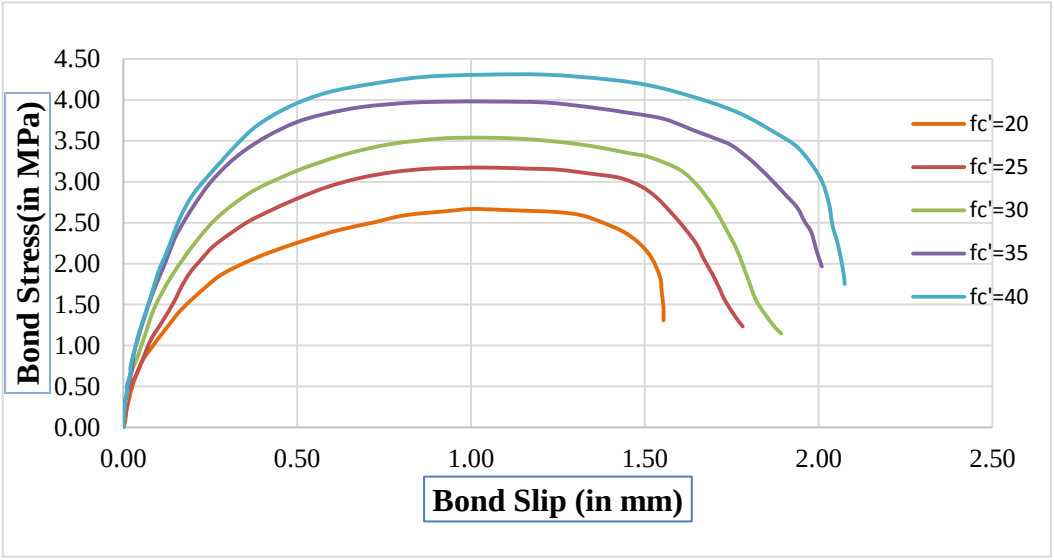


Figure 4-5 Bond stress slip curve of embedment depth L=40mm for varying concrete strength

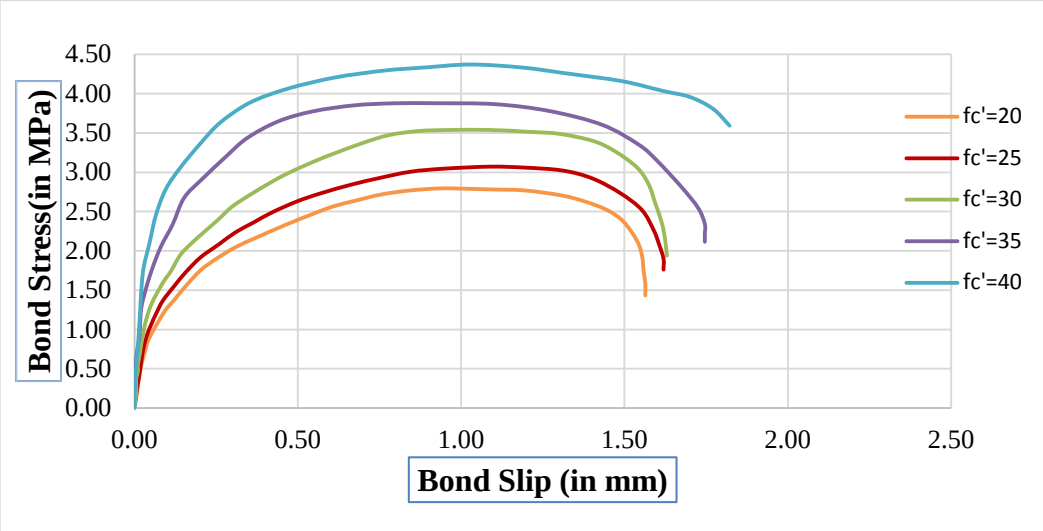


Figure 4-6 Bond stress slip curve of embedment depth L=45mm for varying concrete strength

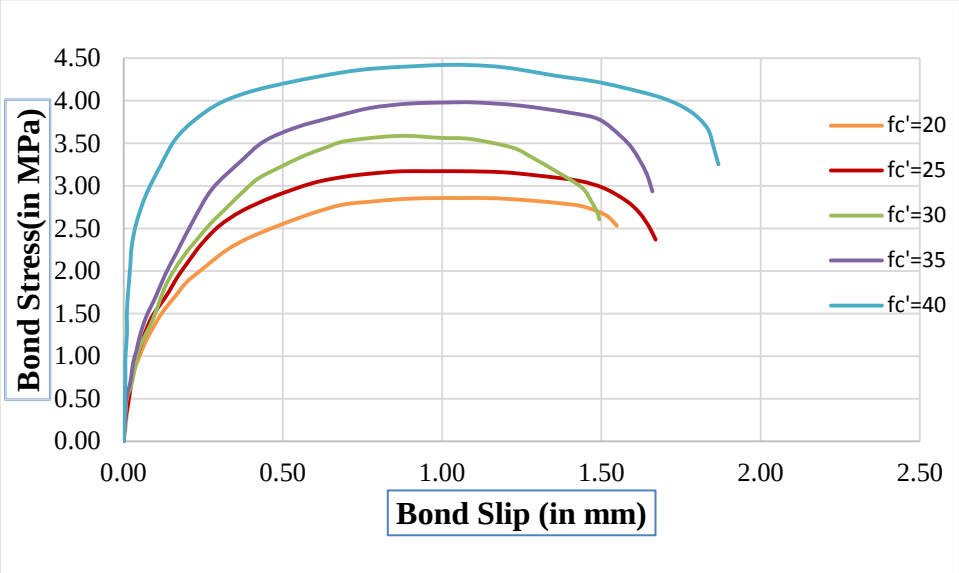


Figure 4-7 Bond stress slip curve of embedment depth L=50mm for varying concrete strength

Figure 4-3 to 4-7 shows relationship of bond stress-slip for different anchorage length under varying concrete strength. Increasing the concrete strength from fc'=20MPa to 40MPa increased the monotonic bond capacity by 50% to 76%. For shorter embedment length the effect of varying concrete strength is significant.

4.2.2 Effect on Bond Stress-Bond Slip Relation Under Low Cycle Fatigue

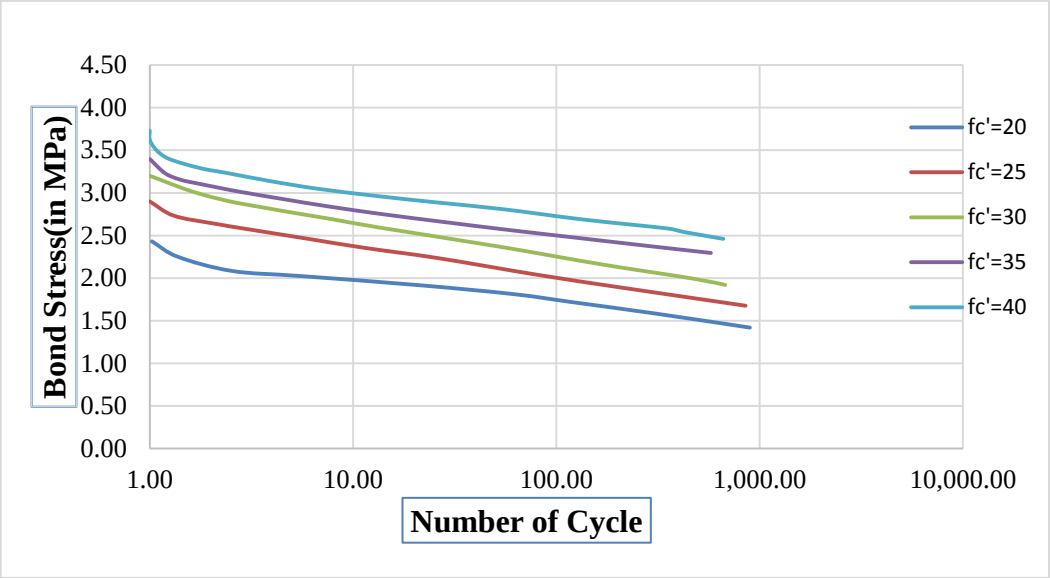


Figure 4-8 S-N curve of short embedment (L=30mm) for varying concrete strength

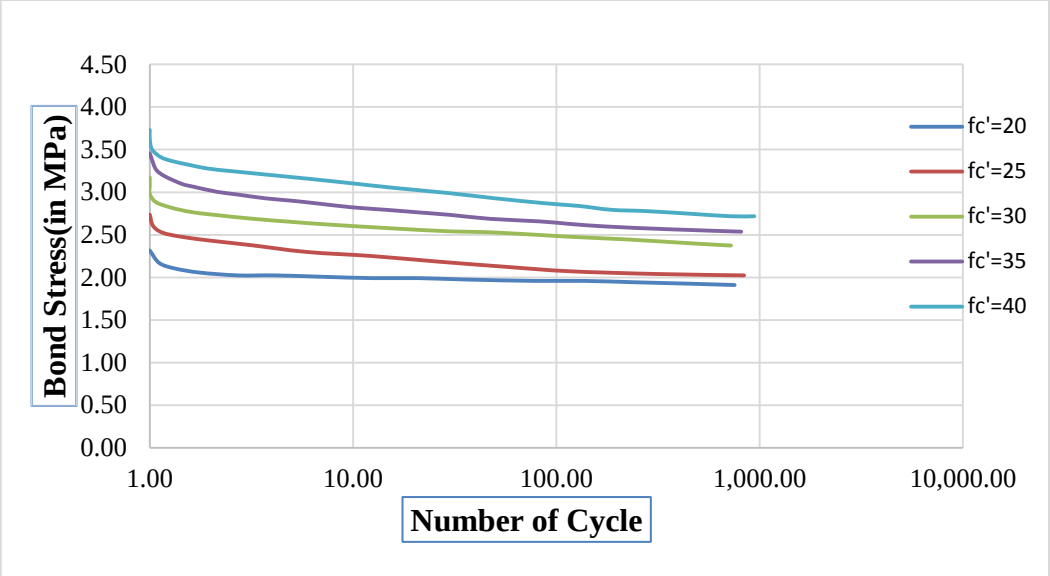


Figure 4-9 S-N curve of long embedment (L=50mm) for varying concrete strength

Figures 4-7 & 4-8 shows bond stress number of cycle curves with concrete strength varied from 20MPa to 40MPa under low cyclic loadings. Clearly the concrete strength has a significant effect on the value of bond strength and the post-peak behavior. It was shown that fatigue life substantially increases while increasing concrete strength.

An explanation of such behavior is found in the progressive deterioration of concrete under fatigue loadings, in addition, increasing concrete strength lead to higher tensile strength and intact behavior.

4.3 Effect of Embedment Length

Another parameter that is of interest is the anchorage length. Sufficient length of embedment of the steel anchorages (l_b) should be provided in order to transfer the required tension force from the surrounding concrete to the steel, or conversely. This section aims to numerically evaluate the influence of embedded bond length (le) of the steel anchorages on their bond behavior. For this purpose, the twenty five FE models were used for the numerical evaluation. The embedment length l_b of 30mm, 35mm, 40mm, 45mm and 50mm were numerically adopted, for different concrete strength.

4.3.1 Effect on Bond Stress-Bond Slip Relation

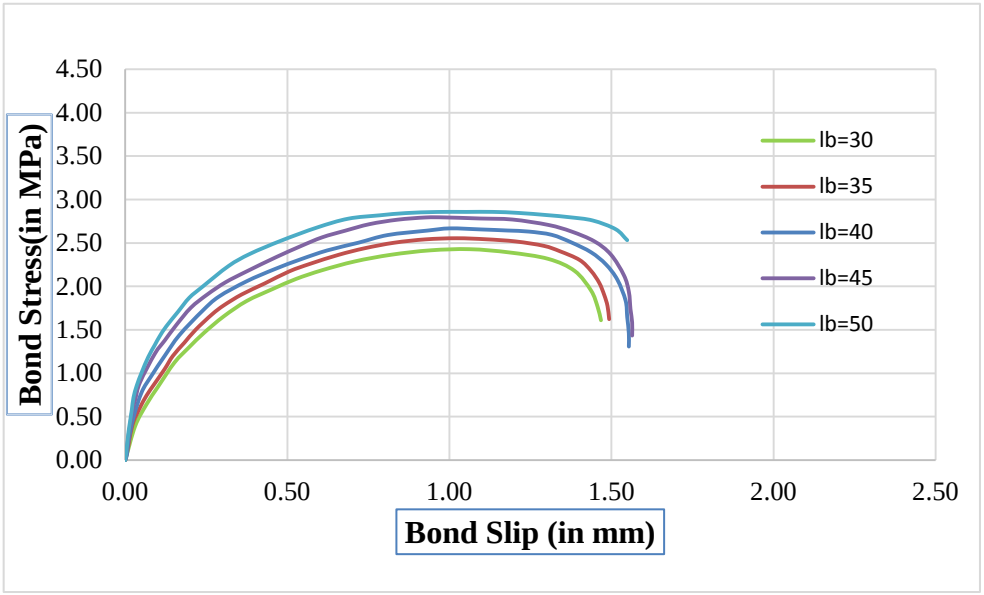


Figure 4-10 Bond Stress-Slip curve for varying embedment (fc'=20MPa)

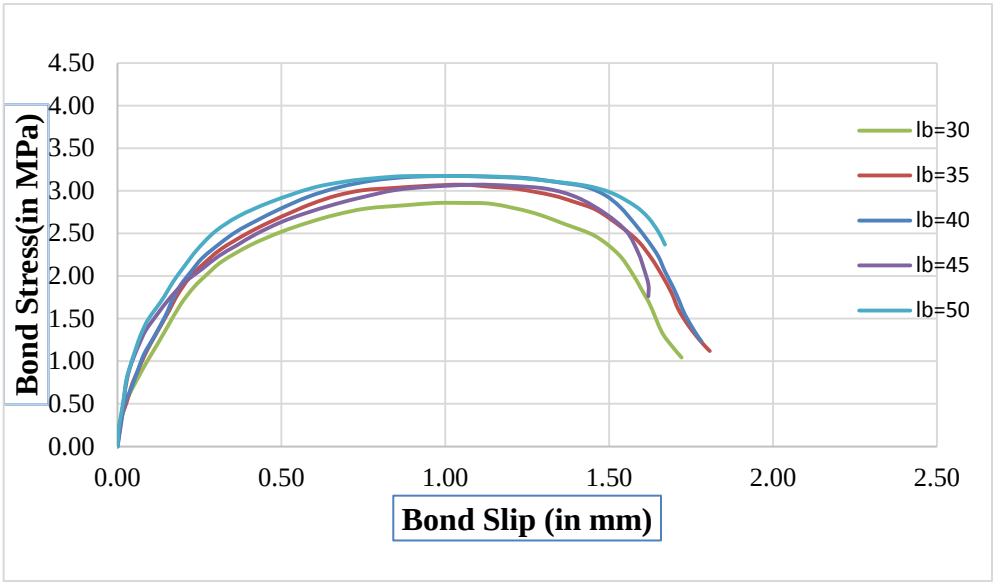


Figure 4-11 Bond Stress-Slip curve for varying embedment (fc'=25MPa)

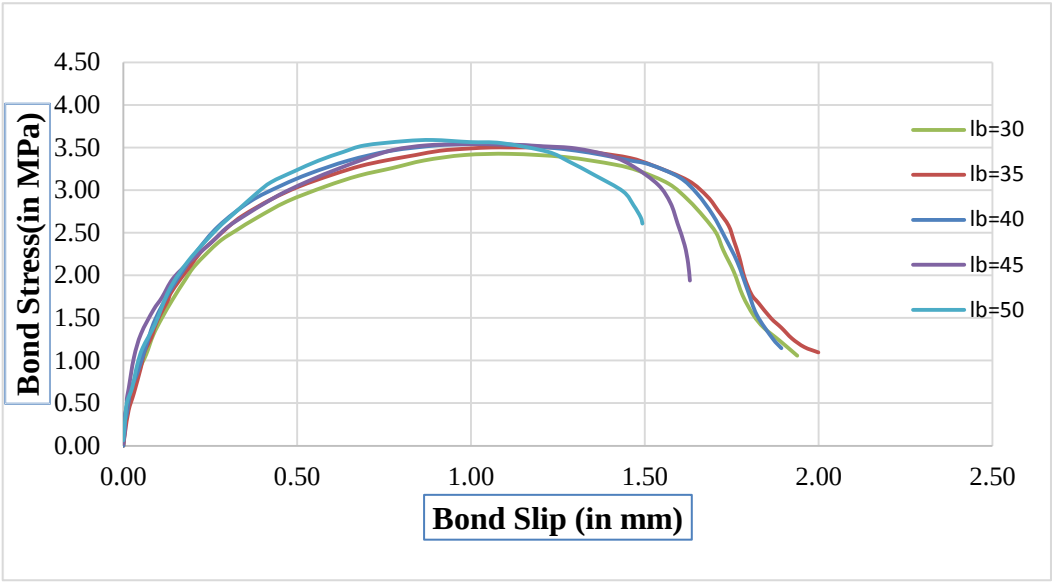


Figure 4-12 Bond Stress-Slip curve for varying embedment (fc'=30MPa)

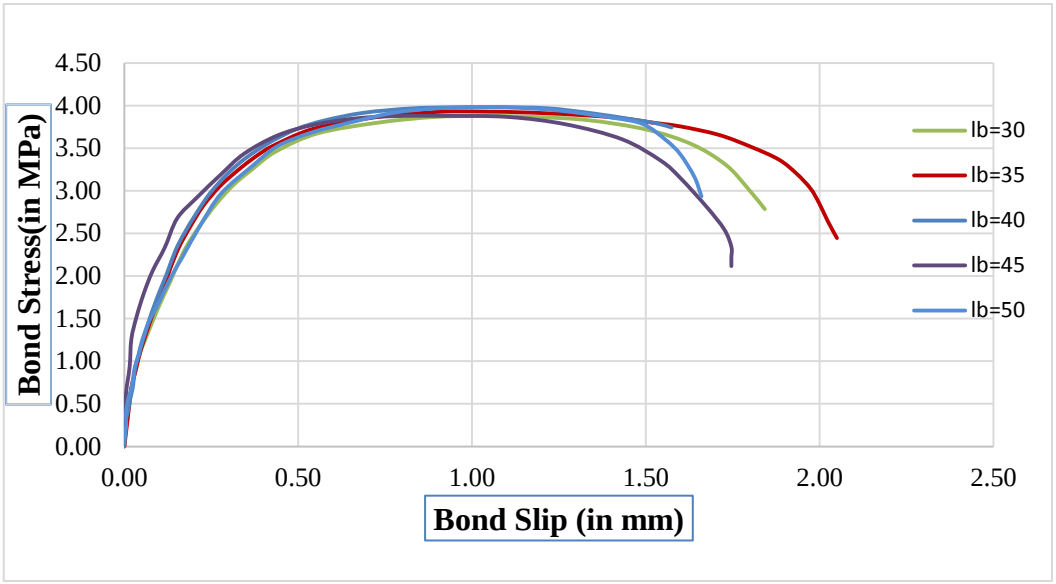


Figure 4-13 Bond Stress-Slip curve for varying embedment (fc'=35MPa)

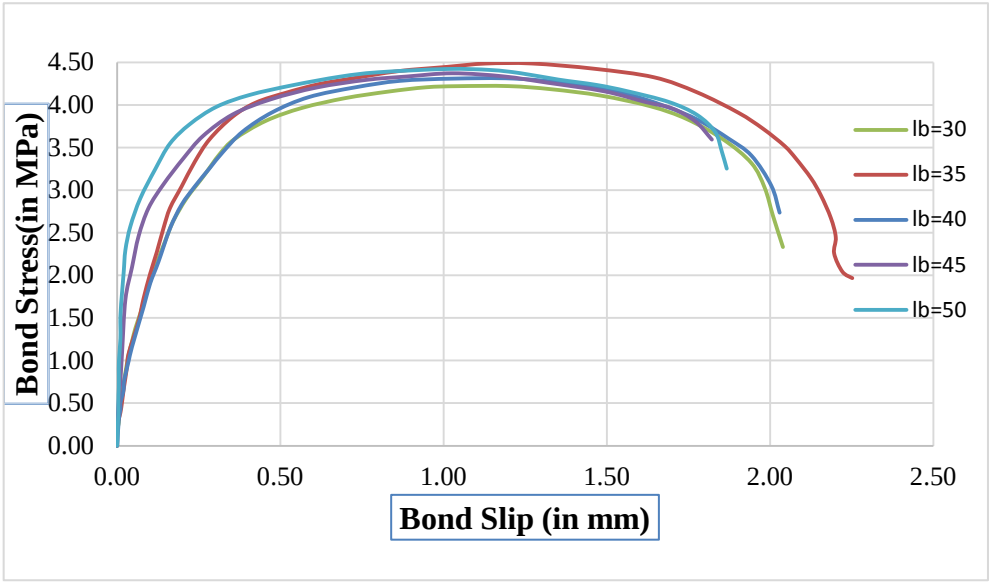


Figure 4-14 Bond Stress-Slip curve for varying embedment (fc'=40MPa)

The numerically estimated bond stress bond slip is shown in Figure 4-10 to 4-13 for different embedded bond lengths. The obtained results showed a similar shape of stress distribution for all the bond lengths. This fact can be attributed to the adopted relatively short range of bond length which is noticeably did not give any sensitive influences upon the bond behavior. Thus the increase in anchorage length did not have much effect in this case.

4.4 Summary on the Effect of Concrete Strength and Embedment Length

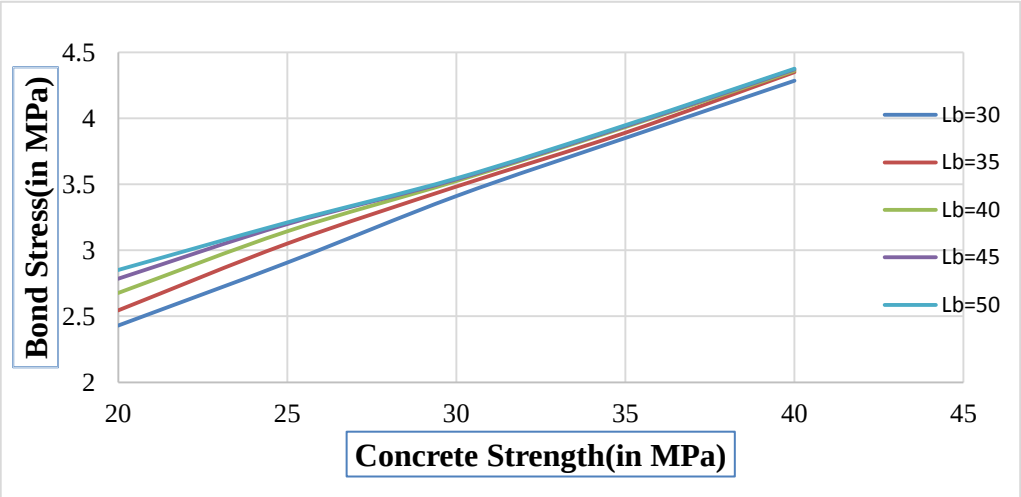


Figure 4-15 Summary of bond strength for varying embedment length

The above figure shows the relationship among bond stress, concrete strength and anchorage depth under monotonic loading. From this the following points have observed;

- as concrete strength increases there is negligible difference in bond strength whilst embedment length is varied.
- for low strength concrete varying embedment length will result in significant increase in bond strength.

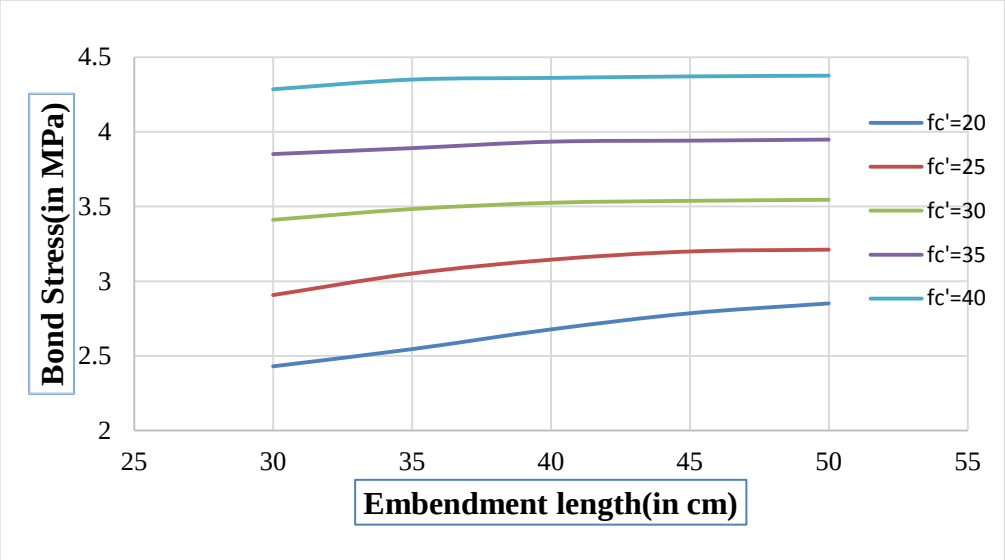


Figure 4-16 Bond stress for varying concrete strength and embedment length

4.5 Bond Stress-Slip Response for Cyclic Slip History

The computed bond stress-slip response for monotonic loading results in a maximum bond stress and the corresponding slip has been taken as a cyclic slip demand to determine the percentage of cyclic loading bond failure compared with the static loading. Here response is characterized by deterioration of bond strength with progressive value of the slip demand. These data is presented in Table 4.1 identify the comparison of maximum fatigue loading required to have the maximum slip value for the corresponding concrete strength.

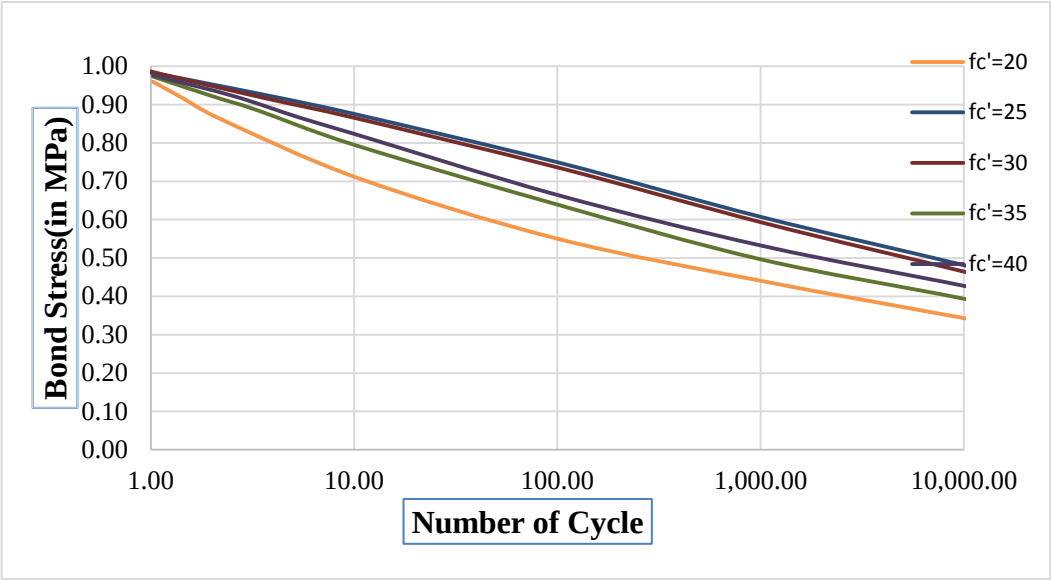
Table 4-1-Maximum bond stress value for monotonic and cyclic slip history

fc'	Maximum Bond Stress Monotonic Slip History	Maximum Bond Stress Cyclic Slip History	Comparison (%)
20	2.826	2.008	71.067
25	3.173	2.311	72.833
30	3.501	2.595	74.122
35	3.929	3.229	82.184
40	4.221	3.778	89.505
		Average	77.942

As illustrated above for the given systems subjected to reversed cyclic slip histories as this slip history bond strength at more extreme slip levels is significantly less than that observed under monotonic loading[around 78%].

4.6 Bond Deterioration

The numerical analysis of concrete-to-steel bond indicates that bond strength deteriorates as the number of load cycles increases. Strength deterioration is represented by a damage parameter, δ, defined as the ratio of the maximum bond strength developed under a cyclic slip history versus that developed under a monotonic slip history. Thus, represents a state of zero damage due to cyclic loading and represents complete damage due to cyclic loading.



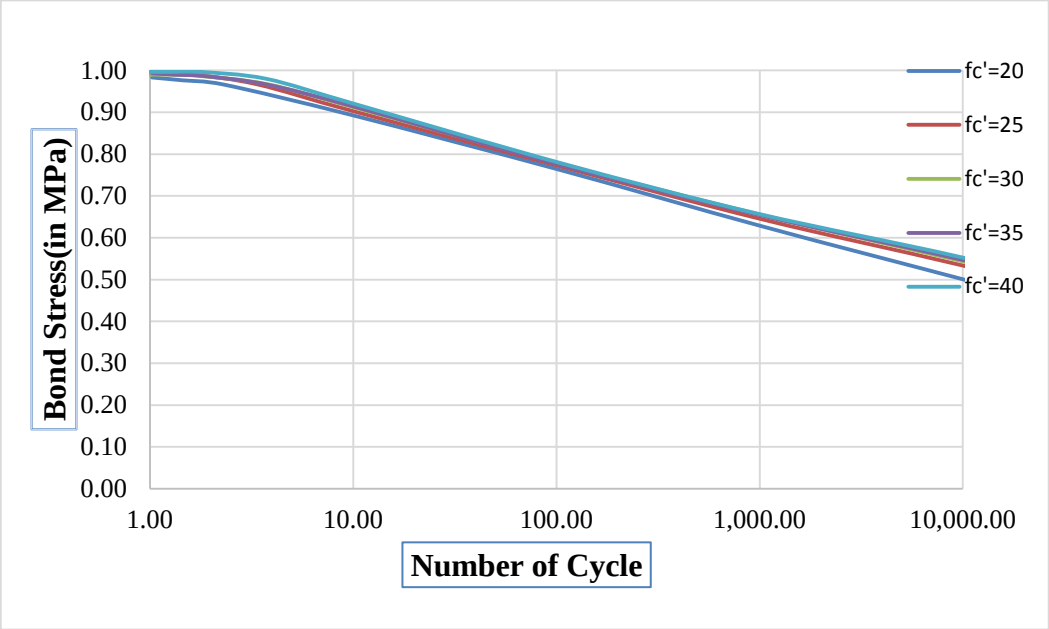


Figure 4-17 Bond degradation curves for varying concrete strength

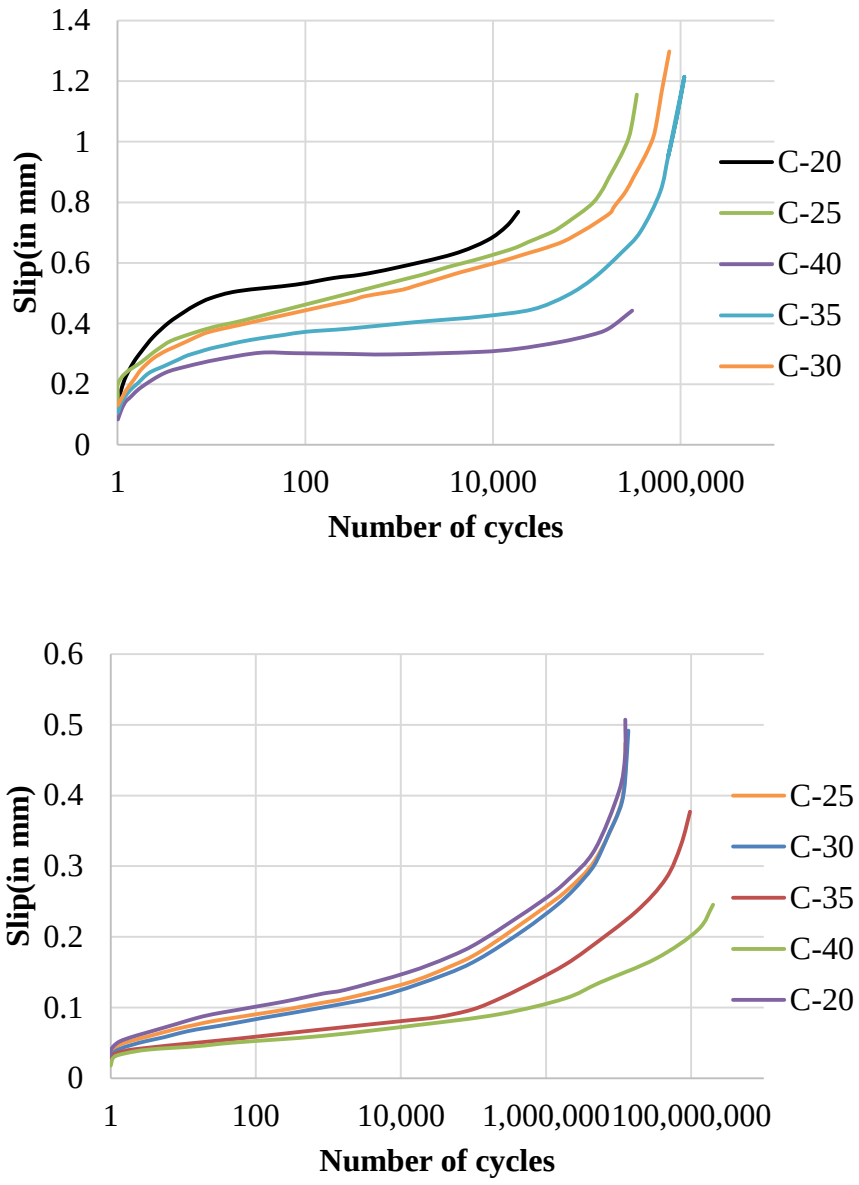


Figure 4-18 Slip-number of cycle curves for varying concrete strength (Short and long embedment length)

The plot of the computed deterioration in bond strength for the series of prescribed slip histories. Figure 4-17 Bond degradation curves for varying concrete strength, defines deterioration of *maximum* bond strength; while the data in Figure 4-18 Slip-number of cycle curves for varying concrete strength show the deterioration of bond strength achieved at a particular maximum slip demand. Here deterioration in maximum bond strength is related to absolute maximum slip demand for systems subjected to one and ten cycles of loading.

4.7 Code Comparison

Comparison of bond strength obtained analytically, according to Eurocode 2, and the results obtained numerically by FE model, is presented on the following figures.

4.7.1 Eurocode Provision for Bond Strength

EN 1992-1-1 provides formulas on bond in relation to anchor lengths. The ultimate bond stress is given by the expression:

Ultimate bond stress:

The design value of the ultimate bond stress, f_{bd}, for ribbed bars may be taken as:

$$f_{bd} = 2.25\eta_1\eta_2 f_{ctd} \tag{4-1}$$

where:

f_{ctd} is the design value of concrete tensile strength

Due to the increasing brittleness of higher strength concrete, $f_{ctk,0.05}$ should be limited here to the value for C60/75, unless it can be verified that the average bond strength increases above this limit

η_1 is a coefficient related to the quality of the bond condition and the position of the bar during concreting

η_1= 1.0 when 'good' conditions are obtained and

η_1= 0.7 for all other cases and for bars in structural elements built with slip-forms, unless it can be shown that 'good' bond conditions exist

η_2 = 1.0 for $\phi \leq 32$ mm

η_2 = (132 - ϕ)/100 for ϕ> 32 mm

Basic anchorage length

The basic required anchorage length, $l_{b,rqd}$, for anchoring the force A_s,σ_{sd} in a straight bar assuming constant bond stress equal to f_{bd} follows from:

$$l_{b,rqd} = (\phi / 4)(\sigma_{sd} / f_{bd}) \tag{4-2}$$

Where σ_{sd} is the design stress of the bar at the position from where the anchorage is measured from. Values for f_{bd} are given in Eq 4.1.

Table 4-2 Bond stress f_{bd} and basic anchorage length $l_{bd,\ reqd}$ for good bond conditions, fyk=400MPa

	f_{bd}		$l_{bd,reqd}$	
f_{ck}	Ø≤ 32 mm	Ø = 40 mm	Ø ≤ 32 mm	Ø = 40 mm
20	2.32	2.13	47	51
25	2.70	2.48	40	44
30	3.05	2.81	36	39
35	3.37	3.10	32	35
40	3.69	3.40	30	32
45	4.00	3.68	27	30
50	4.28	3.94	25	28
55	4.43	4.08	25	27
60	4.57	4.20	24	26

The minimum cover to ensure adequate bond should not be less than the bar diameter, or equivalent bar diameter for bundled bars, unless the aggregate size is over 32 mm.

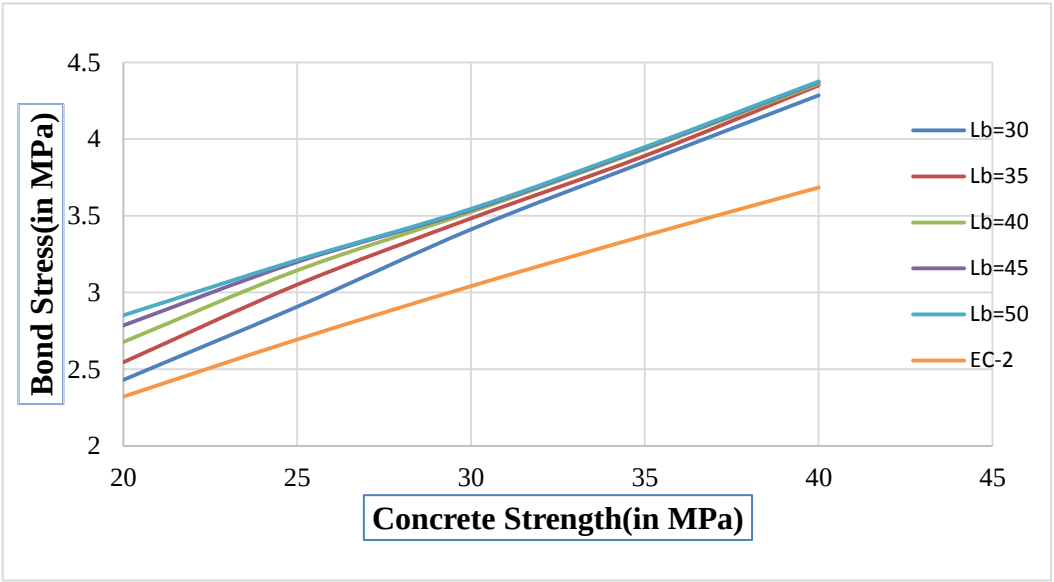


Figure 4-19 EC-2 comparison with numerical results for different embedment length and concrete strength under monotonic loading

EC-2 provide the same bond strength for all length of embedment rather than considering the effect of varying embedded length. Eurocode gives conservative result when compared with numerical results.

Table 4-3 Bond strength of numerical result after different cycles compared to EC-2 provisions (short embedment)

Concrete Strength	Bond Strength			EC-2 Results
	After 10 cycles	After 100 cycles	After 1000 cycles	
20	1.918	1.721	1.238	2.321
25	2.356	1.888	1.465	2.693
30	2.597	2.159	1.812	3.041
35	2.748	2.477	2.220	3.370
40	2.960	2.688	2.477	3.684

Table 4-4 Bond strength of numerical result after different cycles compared to EC-2 provisions (long embedment)

Concrete Strength	Bond Strength				EC-2 Results
	After 10 cycles	After 100 cycles	After 1000 cycles	After 10,000 cycles	
20	1.992	1.960	1.862	1.506	2.321
25	2.251	2.073	1.992	1.895	2.693
30	2.575	2.478	2.380	2.280	3.041
35	2.792	2.630	2.522	2.430	3.370
40	3.051	2.842	2.722	2.701	3.684

CHAPTER 5

5 CONCLUSIONS AND RECOMMENDATIONS

5.1 Conclusions

Conclusions were drawn concerning the effects of adjusting the parameters of the model. The following are some of conclusions that are deduced from the analysis.

1. The proposed finite element model gives a quite accurate prediction for the behaviors of concrete steel connections under low cycle fatigue loadings taking the effect of interface between concrete and steel, compression and tensile softening introducing damage in the concrete material. It proved the rationality of selected element types, constitutive models and contact models. The comparison of those models with experimental results showed that the numerical model gives remarkable result for performing and modeling concrete steel connection to study bond behavior under low cycle load. The finite element software ABAQUS was capable of modeling steel-concrete interface, including the bond-slip behavior experienced between concrete and steel.
2. The results from the bond stress-slip have implied the influence of the concrete strength on the bond stress-slip relationship was large in the tested range (f_c'=20MPa to f_c'=40Mpa). A small adjustment in the concrete strength changes the conditions markedly. But the effect was rather small as embedment length increases. The FE models with higher tensile capacity, i.e., higher concrete strength have a higher ultimate bonding stress.
3. Based on the parameters studied, fatigue loads causes bond failure in the steel-concrete connections subjected to a low cycle loads of as little as 78% of their static capacity. Even for low strength concretes mode of failure has changed to splitting failure. Low cycle fatigue and decreased the bond strength under monotonic loading by 21-23%.
4. Bond deterioration under many cycles (more than 1000 cycles) is high and it can be enhanced by the use of very long anchorage lengths (at least a factor of 1.5 on the development lengths currently used). Even in this case, bond damage near the most highly stressed areas cannot be totally eliminated.
5. EC-2 provision for bond strength is conservative but good agreement is obtained between the provision for development length and the studied numerical model. Development length of steel anchorages provided in code can be safely used and

there is good agreement between results of numerical model. On the other hand the bond strength provided on EC-2 over estimates the bond strength for low cyclic fatigue loading but it is conservative enough to be used for monotonic loading. Cyclic loadings changed the failure mode of the connection to bond failure even though it has sufficient bond length to resist static loadings. So that under cyclic loadings additional anchorage length must be taken.

5.2 Recommendations

This paper focused on bond behaviour under fatigue loading. The conclusions and results are limited by the scope of the study and the parameters that were investigated. It is recommended that additional parameters be conducted to study the bond performance under fatigue loading. Specifically, it is suggested the effect of such variables as the bar diameter, the concrete cover, the confinement effect and the loading effect be studied.

An extensive study is needed to determine the residual bond strength which is very important to determine the remaining service life of deteriorated concrete for the connections with steel.

Experimental tests should be conducted for the parametric values selected to see the accuracy of the numerical models.

In continuing the research concept, the reflections presented in this paper for steel anchors to concrete connection it will serve as the basis to specify design verifications concerning fatigue in reinforced concrete structures regarding bond fatigue.

REFERENCES

1. Eligehausen, R., Popov, E. P., and Bertero, V. V. (1983). "Local bond stress—slip relationships of deformed bars under generalized excitations." UCB/EERC-83/23, Earthquake Engineering Research Center,.
2. ACI Committee 408, 2003, "Bond and Development of Straight Reinforcing Bars in Tension (ACI 408R-03)," American Concrete Institute, David Darwin, ChairHills, Adolfo.
3. Fib-Bulletin No. 102000. Bond of reinforcement in concrete-state of the art report.
4. Murcia-Delso, J., Stavridis, A., and Shing, P. B. (2013). "Bond strength and cyclic bond deterioration of large-diameter bars." ACI Struct. J., 110(4), 659–669.
5. Viwathanatepa, S., Popov, E. P., and Bertero, V. V. (1979). "Effects of generalized loadings on bond of reinforcing bars embedded in confined concrete blocks." Rep. No. UCB/EERC-79/22, .
6. Rehm, G., & Elingehausen, R. (1979, Feb). Bond of ribbed bars under high cycle repeated loads. ACI Journal, Proceedings, 76, 297 - 309.
7. Auyeung, Y., Chung, L., & Balaguru, P. (2000, March). Bond behaviour of corroded reinforced bars. ACI Materials Journal, 97(2), 214 - 220.
8. Balazs, G., & Koch, R. (1992, October). Influence of load history on bond behaviour. Proceedings: and -. Bond in concrete - from research to practice.
9. Ngo D., S.A.C., Finite element analysis of reinforced concrete beams, 1967, ACI Journal, No. 14, PP. 152-163.
10. Balazs, G., Nov - Dec). Fatigue of bond. ACI Materials Journal, 88(6), 620 – 629.
11. Bamonte, P., & Gambarova, P. (2007). High-Bond Nars in NSC and HPC: Study on Size Effect and on the Local Bond Stress-Slip Law. Journal of Structural Engineering, 133, 225 – 234.
12. ACI Committee 408. (2003). Bond and Development of Straight Reinforcing Bars in Tension (ACI 408R-03). Farmington Hills, M.A.C.I.
13. Khalfallah, S.a.O., M., A Numerical Simulation of Bond for PullOut Tests: The Direct Problem, 2007, Asian Journal of Civil Engineering (Building and Housing) Vol. 8, No. 5, Pages 491-505.
14. Abaqus V. 6.10 [Computer software]. Dassault Systemes Simulia Corp., P., RI.

15. Ožbolt, J., Lettow, S. and I. Kožar., Discrete Bond Element For 3d Finite Element Analysis Of Reinforced Concrete Structures, 2002.
16. Cox, J.V., and Herrmann, L. R. (1998). "Development of a plasticity bond model for steel reinforcement." Mech. Cohesive-Frict. Mater., 3(2), 155–180.
17. Al-Hammoud, R., Soudki, K., & Topper, T. (2010, March). Bond Analysis of Corroded Reinforced, Concrete Beams Under Monotonic and Fatigue Loads. Cement and Concrete Composites, and -. 32(3).
18. Khalfallah, S., Tension Stiffening Bond Modelling Of Cracked Flexural Reinforced Concrete Beams, 2008, Journal of Civil Engineering and Management, pp. 131-137.
19. Rteil, A., Soudki, K., & Topper, T. (2011). Mechanics of Bond Under Repeated Loading. and Construction and Building of Materials, 2822 - 2827.
20. Bresler, B., & Bertero, V. (1968, June). Behaviour of reinforced concrete under repeated loading. and ASCE Journal of Structural Division, 1567 - 1589.
21. Shafaie, J., Hosseini, A. and Marefat, M.S., (2009), 3D Finite Element Modeling of Bond-Slip Between Rebar and Concrete in Pull-Out Test, The 3rd International Conference on Concrete and Development, Tehran, I.R. Iran.
22. Shima, H.C., L.-L.; Okamura, H. (1987): Micro and macro models for bond in reinforced concrete. Journal of the Faculty of Engineering, Vol. XXXIX, No. 2, 133-194, University of Tokyo.
23. Hsu, L.S., & Hsu, C.-T.T. (1994) Complete stress-strain behaviour of high-strength concrete under compression. Magazine of Concrete Research, 46(169), 301-312.
24. Youai, G., Bond Stress and Slip Modeling in Nonlinear Finite Element Analysis of Reinforced Concrete Structures, 2000, MSc thesis, Department of Civil Engineering, The University of Toronto, Canada.
25. Rteil, A., Soudki, K., & Topper, T. (2007). Confinement effect of CFRP sheets on the bond between concrete and steel subjected to repeated loading. 8th Interantional Symposium on FRP and G.F.-. Reinforcement for Concrete Structures (p. on CD ROM). Patras.
26. Lettow, S., Eligehausen, R., The Simulation of Bond between Concrete and Reinforcement in Nonlinear Three-dimensional Finite Element Analysis, 2003, IWB, University of Stuttgart, Stuttgart, Germany.

27. Cho, J.Y., and Pincheira, J. A. (2006). "Inelastic analysis of reinforced concrete columns with short lap splices subjected to reversed cyclic loads." ACI Struct. J., 103(2), 280–290.

28. Guizani, L., & Chaallal, O. (2011). An Experimental Study on Bond-Slip in Moderately Confined, C.S.t.M.a.C.L.U.a.E.P. Cnadian, and Journal in Civil Engineering, 272 - 282.

29. EN 1992. Eurocode 2: Design of Concrete Structures, Part 1–1: General Rules and Rules for Buildings; European Committee for Standardization (CEN): Brussels, Belgium, 2005

APPENDIX A

Abaqus Script File

*Heading

** Job name: Job-3 Model name: From D

** Generated by: Abaqus/CAE 6.14-2

*Preprint, echo=NO, model=NO, history=NO, contact=NO

**

** PARTS

**

*Part, name=Part-1

*Node

1, -0.0625, 0.1175, 0.

2, 0.0625, 0.1175, 0.

3, 0.0625, 0.0500000007, 0.

4, -0.0524999984, 0.0500000007, 0.

5, -0.0625, 0.0599999987, 0.

6, 0.0625, 0.1175, 0.25

7, -0.0625, 0.1175, 0.25

8, -0.0625, 0.0599999987, 0.25

9, -0.0524999984, 0.0500000007, 0.25

10, 0.0625, 0.0500000007, 0.25

11, -0.0625, 0.174999997, 0.

*Elset, elset=_concsurf_S4, internal

69, 74, 79, 178, 183, 188, 287, 292, 297, 396, 401, 406, 505, 510, 515, 614

619, 624, 723, 728, 733, 832, 837, 842, 941, 946, 951, 1050, 1055, 1060, 1159, 1164

1169, 1268, 1273, 1278, 1377, 1382, 1387, 1486, 1491, 1496, 1595, 1600, 1605, 1704, 1709,

1813, 1818, 1823, 1922, 1927, 1932, 2031, 2036, 2041, 2140, 2145, 2150, 2249, 2254, 2259,

2363, 2368, 2467, 2472, 2477, 2576, 2581, 2586, 2685, 2690, 2695, 2794, 2799, 2804, 2903,

2913, 3012, 3017, 3022, 3121, 3126, 3131, 3230, 3235, 3240, 3339, 3344, 3349, 3448, 3453,

3557, 3562, 3567, 3666, 3671, 3676, 3775, 3780, 3785, 3884, 3889, 3894, 3993, 3998, 4003,

4107, 4112, 4211, 4216, 4221, 4320, 4325, 4330, 4429, 4434, 4439, 4538, 4543, 4548, 4647,

4657, 4756, 4761, 4766, 4865, 4870, 4875, 4974, 4979, 4984, 5083, 5088, 5093, 5192, 5197,

5301, 5306, 5311, 5410, 5415, 5420, 7920, 7925, 7930, 8025, 8030, 8035, 8130, 8135, 8140,

8240, 8245, 8340, 8345, 8350, 8445, 8450, 8455, 8550, 8555, 8560, 8655, 8660, 8665, 8760,

8770, 8865, 8870, 8875, 8970, 8975, 8980, 9075, 9080, 9085, 9180, 9185, 9190, 9285, 9290,

9390, 9395, 9400, 9495, 9500, 9505, 9600, 9605, 9610, 9705, 9710, 9715, 9810, 9815, 9820,

9920, 9925, 10020, 10025, 10030, 10125, 10130, 10135, 10230, 10235, 10240, 10335, 10340, 10345, 10440, 10445

10450, 10545, 10550, 10555, 10650, 10655, 10660, 10755, 10760, 10765, 10860, 10865, 10870, 10965,

11070, 11075, 11080, 11175, 11180, 11185, 11280, 11285, 11290, 11385, 11390, 11395, 11490, 11495,

11600, 11605, 11700, 11705, 11710, 11805, 11810, 11815, 11910, 11915, 11920, 12015, 12020, 12025, 12120, 12125

12130, 12225, 12230, 12235, 12330, 12335, 12340, 12435, 12440, 12445, 12540, 12545, 12550, 12645, 12650, 12655*Elset, elset=_Surf-8_S2, internal, instance=Part-2-1

393, 394, 395, 396, 397, 398, 399, 400, 793, 794, 795, 796, 797, 798, 799, 800

*Elset, elset=_Surf-8_S5, internal, instance=Part-1-1

6039, 6040, 6041, 6042, 6043, 6044, 6639, 6640, 6641, 6642, 6643, 6644, 7239, 7240, 7241,

7243, 7244, 7839, 7840, 7841, 7842, 7843, 7844, 13594, 13595, 13596, 13597, 13598, 13599,

14095, 14096, 14097, 14098, 14099, 14100, 14594, 14595, 14596, 14597, 14598, 14599, 14600, 15094,

15097, 15098, 15099, 15100

*Elset, elset=_Surf-8_S3, internal, instance=Part-1-1

6045, 6046, 6047, 6048, 6049, 6050, 6645, 6646, 6647, 6648, 6649, 6650, 7245, 7246, 7247, 7248

7249, 7250, 7845, 7846, 7847, 7848, 7849, 7850

*Elset, elset=_Surf-8_S4, internal, instance=Part-1-1

13591, 13592, 13593, 14091, 14092, 14093, 14591, 14592, 14593, 15091, 15092, 15093

*Surface, type=ELEMENT, name=Surf-8

_Surf-8_S2, S2

_Surf-8_S5, S5

_Surf-8_S4, S4

_Surf-8_S3, S3

*Elset, elset=_Surf-11_S2, internal, instance=Part-1-1*Elset, elset=_Surf-11_S2, internal, instance=Part-2-1

393, 394, 395, 396, 397, 398, 399, 400, 793, 794, 795, 796, 797, 798, 799, 800

*Elset, elset=_Surf-11_S5, internal, instance=Part-1-1

6039, 6040, 6041, 6042, 6043, 6044, 6639, 6640, 6641, 6642, 6643, 6644, 7239, 7240, 7241,

7243, 7244, 7839, 7840, 7841, 7842, 7843, 7844, 13594, 13595, 13596, 13597, 13598, 13599,

14095, 14096, 14097, 14098, 14099, 14100, 14594, 14595, 14596, 14597, 14598, 14599, 14600, 15094,

15097, 15098, 15099, 15100

*Elset, elset=_Surf-11_S3, internal, instance=Part-1-1

6045, 6046, 6047, 6048, 6049, 6050, 6645, 6646, 6647, 6648, 6649, 6650, 7245, 7246, 7247, 7248

7249, 7250, 7845, 7846, 7847, 7848, 7849, 7850

*Elset, elset=_Surf-11_S4, internal, instance=Part-1-1

13591, 13592, 13593, 14091, 14092, 14093, 14591, 14592, 14593, 15091, 15092, 15093

*Surface, type=ELEMENT, name=Surf-11

_Surf-11_S2, S2

_Surf-11_S5, S5

_Surf-11_S4, S4

_Surf-11_S3, S3

*Elset, elset=_Surf-12_S2, internal, instance=Part-2-1

393, 394, 395, 396, 397, 398, 399, 400, 793, 794, 795, 796, 797, 798, 799, 800

*Surface, type=ELEMENT, name=Surf-12

_Surf-12_S2, S2

*End Assembly

** MATERIALS

*Material, name=Concrete

*Density 2380.,

*Elastic 2.5e+10, 0.2

*Concrete Damaged Plasticity

31., 0.1, 1.16, 0.667, 0.

*Concrete Compression Hardening

2.56e+07, 0.

3e+07, 8e-05

3.36e+07, 0.00016

3.64e+07, 0.000266667

3.84e+07, 0.0004

3.96e+07, 0.00056

4e+07, 0.000746667

3.96e+07, 0.00096

3.84e+07, 0.0012

3.64e+07, 0.00146667

3.36e+07, 0.00176

3e+07, 0.00208

2.56e+07, 0.00242667

2.04e+07, 0.0028

1.44e+07, 0.0032

7.6e+06, 0.00362667

*Concrete Tension Stiffening

4e+06, 0.

40000., 0.00133333

*Concrete Compression Damage, tension recovery=0.08

0., 0.

0., 2.67e-05

0., 8e-05

0., 0.00016

0., 0.000266667

0., 0.0004

0., 0.00056

0., 0.000746667

0.01, 0.00096

0.04, 0.0012

0.09, 0.00146667

0.16, 0.00176

0.25, 0.00208

0.36, 0.00242667

0.49, 0.0028

0.64, 0.0032

0.81, 0.00362667

*Concrete Tension Damage, compression recovery=0.85

0., 0.

0.99, 0.00133333

*Material, name=steel

*Density 7480.,

*Elastic 2.1e+11, 0.2

*Plastic 2e+08, 0.

2.46e+08, 0.0237

2.94e+08, 0.0478

3.74e+08, 0.0944

4.37e+08, 0.139

4.8e+08, 0.181

4.8e+08, 0.2

4.8e+08, 0.215

** INTERACTION PROPERTIES

*Surface Interaction, name=IntProp-11.,

*Friction, slip tolerance=0.005 0.8,

*Cohesive Behavior, REPEATED CONTACTS

1.5e+12, 3.6e+11, 3.6e+11

*Damage Initiation, criterion=MAXS

4.5e+08, 3e+08, 3e+08

*Damage Evolution, type=ENERGY, mixed mode behavior=POWER LAW, power=1.45

0.09, 0.9, 0.9

** BOUNDARY CONDITIONS

** Name: BC-1 Type: Symmetry/Antisymmetry/Encastre

*Boundary

Set-3, XSYMM

** INTERACTIONS

** Interaction: Int-1

*Contact Pair, interaction=IntProp-1, small sliding, type=SURFACE TO SURFACE, adjust=0.0

Part-1-1.concsurf, Part-2-1.steelsurf

** STEP: Step-1

*Step, name=Step-1, nlgeom=NO, inc=1000

*Static

0.01, 1., 1e-45, 0.02

** BOUNDARY CONDITIONS

** Name: BC-2 Type: Displacement/Rotation

*Boundary

Set-7, 1, 1

Set-7, 2, 2

Set-7, 3, 3

** LOADS**

** Name: Load-1 Type: Pressure

*Dsload

Surf-12, P, -3e+07

** OUTPUT REQUESTS

*Restart, write, frequency=0

** FIELD OUTPUT: F-Output-1

*Output, field

*Node Output

CF, PHILSM, PSILSM, RF, U

*Element Output, directions=YES

DAMAGEC, DAMAGET, LE, PE, PEEQ, PEMAG, S

*Contact Output

CDISP, CSTRESS

** HISTORY OUTPUT: H-Output-1

*Output, history, variable=PRESELECT

*End Step